# Non-linear dendritic integration in frontal circuits shapes sensory discrimination in rodents

Mattia Aime[1,3,#] , Elisabete Augusto[1,3], Vladimir Kouskoff[1,3], Christelle Martin[1,2,3], Yann Humeau[1,3], Nicolas Chenouard[1,3], and Frédéric Gambino[1,3*]

[1] Interdiscliplinary Institute for NeuroScience (IINS), Centre Broca Nouvelle-Aquitaine, 146, rue Léo-Saignat, 33076 Bordeaux, France.

[2] Pole In Vivo.

[3] UMR5297 CNRS and University of Bordeaux.

*, Corresponding Author: Frédéric Gambino (frederic.gambino@u-bordeaux.fr)

#, Present address: University of Bern, Department of Neurology, Inselspital University Hospital Bern, Freiburgstrasse 18, CH-3010 Bern, Switzerland

Number of figures: 7

Number of Supplementary figures: 4

Number of Supplementary tables: 1

Number of words: Title: 11, Abstract: 137, Main text: 4927; Methods: 2770

## ABSTRACT

Survival critically depends on the ability of animals to select the appropriate behavior in response to threat and safety signals from the external world. However, the synaptic and circuit mechanisms by which the brain learns to encode accurate predictors from noise remain largely ignored. Here, we show that frontal association cortex (FrA) dendrites discriminate auditory modalities through the recruitment of non-linear, NMDARs-dependent conductances. These active dendrites can further modify membrane potential dynamics by specifically integrating auditory cues and basolateral amygdala (BLA) inputs. This cooperative mechanism critically shapes the expression of safety *vs.* fear memories generated from sensory cues that were not explicitly paired to an aversive event (*e.g.*, a footshock) during fear conditioning. Taken together, our data reveal a dendritic mechanism for cue discrimination in FrA, thus providing a new framework for discriminative learning and related disorders.

## INTRODUCTION

Discriminative learning is an important survival strategy that depends on the repeated contingency and contiguity between sensory cues (conditioned stimuli, CS) and the events (*e.g.,* danger, safety) that they must predict (unconditioned stimuli, US)[1]. Discriminative learning has been classically studied by using differential fear conditioning paradigms where two different auditory CSs are positively (CS+) and negatively (CS-) paired in time with an aversive US (*e.g.*, foot shock). This learning protocol is supposed to assign appropriate emotional valence to the two incoming CSs[1–3], thereby providing an accurate representation of the environment by increasing discriminative skills between threat and safety signals. While CS+ promotes conditioned fear responses (*e.g.*, freezing behavior) when presented alone, CS- has been shown to serve as a learned safety predictor by reducing fear behavior and increasing positive affective response[4]. Previous work has thoroughly investigated how the CS+ generate fear responses[5,6]. However, it remains unclear how the brain learns to encode CS- and thus discriminates between threat and safety.

The medial prefrontal cortex (mPFC) appeared over the past decade as a critical region that shapes behaviors in response to both aversive and non-aversive environmental cues[3,7,8]. These antagonistic effects of the mPFC possibly develop through specific interaction between its different subdivisions (*i.e.*, prelimbic (PL) and infralimbic (IL) cortices) and the basolateral complex of the amygdala (BLA)[9–11]. However, the mPFC does not receive direct sensory information neither from sensory cortical areas nor from the thalamus[12], thereby supporting the idea that a higher-order neuronal network above the mPFC might encode opposing memories that are later preferentially selected during recall together with its downstream cortical (*e.g.,* PL or IL mPFC) or subcortical structures (*e.g.,* BLA). Specifically, the superficial frontal association cortex (FrA) has been shown to contribute to memory formation during associative learning[13–15]. This region of the lateral part of the agranular cortex (AGl)[16,17] receives inputs from the BLA[13,14,18] and sensory cortices[12,19], and is non-reciprocally connected to the PL/IL subdivisions of the mPFC[19], raising the possibility that it may function as a relay station during learning from sensory cortical areas and the BLA to the mPFC. However, whether and how FrA integrates the variety of sensory information required for discriminative learning is not understood.

The implication of FrA in auditory fear conditioning has constantly been reported. For example, the pharmacological inactivation of FrA neurons alters both the expression and extinction of learned fear[13–15]. Recently, fear conditioning and extinction have been shown to induce in FrA dendritic spine elimination and formation, respectively[13]. Importantly, this phenomenon occurs within the same dendritic branch supporting the idea that a unique FrA circuit could form distinct memory traces with opposing emotional values. Nonetheless, no previous evidence has demonstrated a contribution of the FrA in the encoding of incoming sensory cues as threat or safety predictors and, if so, how such process may be controlled by inputs from the BLA.

To address the possible role of the FrA during discriminative learning and the mechanisms behind it, we explored the dynamics of layers II/III FrA pyramidal neurons and long-range projections from the BLA during the acquisition and recall of discriminative memory traces by using two-photon (2P) calcium imaging in head-restrained mice, *in vivo* whole cells recordings and optogenetic conditional strategies. We found that auditory tones produced *N*-methyl-D-aspartate receptors (NMDARs)-dependent, dendritic plateau-like depolarizations that potentiated FrA L2/3 neurons when combined with the channelrhodopsin-2-mediated activation of BLA neurons projecting to the FrA. During conditioning, those long-range projecting BLA neurons conveyed integrated information about the CS/US association that were critical to CS- *vs.* CS+ discriminative learning. In conclusion, our study reveals a potent dendritic mechanism for encoding cue discrimination in FrA, and thus extends the cortical framework of discriminative learning and related disorders.

## RESULTS

### Auditory stimulation generates dendritic NMDARs-dependent plateau potentials

We first sought to characterize FrA L2 pyramidal cells activation by two widely used forms of auditory stimulations (pure tone *vs*. broad-band mixture of pure tones (white Gaussian noise)), and performed somatic whole-cell recordings in anesthetized naive animals (**Fig. 1**). Consistent with previous *in vivo* recordings of L2/3 pyramidal neurons during anesthesia[20], membrane potential spontaneously fluctuated between up and down-states (**Fig. 1b**). For each recorded cell, postsynaptic potentials (PSP) were monitored prior, during and after the random presentation of both tones, each consisting of 27 pure (8 kHz)-tone or white noise pips (50 ms, 0.9 Hz for 30 s) (**Fig. 1c-f**). To reduce the variability related to spontaneous activity and detect any change in membrane potential that might be specifically induced by auditory stimulation, we computed the cumulative PSPs (cPSP) over time that were then subtracted to the linear regression calculated during the baseline period prior to auditory stimulation (cPSP change) (**Fig. 1c, d**). In contrast to a pure, unpaired (up) sine auditory tone (*up8kHz*) that failed to affect frontal pyramidal neurons activity, unpaired white Gaussian noise (*upWGN*) alone evoked a long-lasting subthreshold depolarization in naive animals (*upWGN*: 27.6 ± 4 mV, *up8kHz*: 1.2 ± 4 mV; n=22, p<0.001, paired t-test) that lasted for at least 30 sec after the end of the stimulation (*upWGN*: 32.5 ± 5 mV, *up8kHz*: -3.8 ± 3 mV; n=22, p<0.001, paired t-test) (**Fig. 1c-f**).

The *upWGN*-evoked increase in cumulative potential (**Fig. 1e**) was similar to evoked cortical up-states which were shown to depend on the activation of NMDA receptors (NMDARs)[21]. In agreement, the sustained depolarization evoked by the *upWGN* was efficiently suppressed by both the topic application of the specific NMDAR antagonist D(-)-2-Amino-5-phosphonovaleric acid (dAP5; 1 mM) or the presence of the NMDAR open-channel blocker MK-801 (1 mM) inside the intracellular solution (iMK801; end of the stimulation; control: 27.6 ± 4 mV, n=22; +dAP5: -13.4 ± 5 mV, n=14; +iMK801: -2.2 ± 2 mV, n=5; p<0.001, *anova*; 30 sec later; control: 32.5 ± 5 mV, n=22; +dAP5: -8.2 ± 4 mV, n=14; +iMK801: -7.7 ± 10 mV, n=5; p<0.001, *anova*) (**Fig. 1e and Supplementary Fig. 1**). As a consequence, the difference between *upWGN*- and *up8kHz*-evoked depolarizations disappeared upon pharmacological blockade of NMDARs (dAP5 and iMK801 conditions pooled together, *upWGN*: -10.5 ± 3.6 mV, n=19; *up8kHz*: -18.2 ± 2.9 mV, n=15; p=0.125, *t-test*). Moreover, both *upWGN* and *up8kHz* hyperpolarized

pyramidal neurons when NMDARs conductances were indifferently blocked by using dAP5 or iMK801 (**Fig. 1e, f**), indicating that this effect is cell-autonomous and unlikely to be due to a network wide modification of the balance between excitation and inhibition. Rather, it potentially exposed the existence of a tone non-specific feed-forward inhibitory circuit. Importantly, it indicates that *up8kHz* was also able to recruit NMDARs conductances, but to a lesser extent than *upWGN.*

The above results suggest that *upWGN*-evoked sustained depolarizations recorded at the soma were cell-autonomous and likely to be mediated by local dendritic $Ca^{2+}$ events through the recruitment of distal NMDARs-dependent conductances that spread towards the soma[21,22]. To test this hypothesis, we infected mice with an AAV9-Syn-flex-GCaMP6s together with a 1:10000 dilution of AAV1-hSyn-cre (**Fig. 2a**) in order to obtain a sparse labeling with only a limited number of GCaMP6s-expressing dendrites. Thus, the activity of 104 isolated, non-overlapping distal dendritic branches was imaged in superficial layer 1 through a chronically-implanted cranial window in awake mice (**Fig. 2b**). We then segregated calcium transients based on their spatial spread along individual dendrites (**Fig. 2c and Supplementary Fig. 2**). Multiple local (full width at half maximum (fwhm) < 50µm) and global (fwhm ≥ 50µm) calcium transients occurred both spontaneously (*i.e.* during baseline prior to stimulation) and upon auditory stimulations (**Fig. 2b-d**). While the full width at half maximum of these local events (21.7 ± (s.d.) 13 µm, n=670 events) fell into the spatial range of NMDA spikes[21,22], global events presumably resulted from backpropagating action potentials (**Fig. 2d**).

Interestingly, the presentation of *upWGN* evoked more local events (Baseline, local: 79, global: 43; *upWGN*, local: 338, global: 98; *up8kHz,* local: 253, global: 86), with a number of local dendritic events per dendrite significantly higher as compared to the presentation of *up8kHz* (baseline: 0.59 ± 0.13; *upWGN*: 3.37 ± 0.3; *up8kHz*: 2.49 ± 0.2; $p<0.001$, *anova*) (**Fig. 2e**). Nevertheless, *up8kHz* generated more local events as compared to baseline, which is in agreement with the effect of NMDARs block on *upWGN*-induced somatic cPSP change observed during anesthesia (see **Fig. 1f**).

Altogether, our results suggest that FrA pyramidal neurons are capable to discriminate auditory stimuli based on their spectral properties during both anesthesia and wakefulness. This occurs at the subthreshold level, with Gaussian auditory tones being more efficient in producing local, dendritic plateau potentials within the same dendritic branch as compared to pure tones.

## Co-activation of segregated BLA and auditory inputs potentiated FrA L2/3 pyramidal neurons

The activation of BLA neurons instructs prefrontal circuits during learning and memory recall[8,14,23]. However, the optical activation of the BLA alone is not sufficient to produce learned associations[24]. Therefore, we hypothesized that BLA axons, along with the synaptic non-linearities evoked by auditory tones, could control L2/3 FrA pyramidal neurons through their projections into L1[25]. To address this question, we expressed the recombinant light-gated ion channel *channelrhodopsin*-2-YFP (ChR2; AAV9-CamKIIa-hChR2-eYFP) into the BLA and performed intracellular recordings in 14 L2/3 FrA neurons from 6 naive mice (**Fig. 3**).

First, we confirmed that BLA neurons projected to the superficial layer 1 of the ipsilateral FrA (<150µm) (**Fig. 3a-c**), thereby most likely contacting dendrites of L2/3 pyramidal neurons. In addition, local photostimulation of ChR2-BLA axons in acute slices produced excitatory postsynaptic current (EPSC) in FrA pyramidal neurons with short latencies (3.5 ± 0.36 ms, n=9) and low jitter (0.289 ± 0.04 ms, n=9), suggesting that a fraction of BLA neurons are monosynaptically connected to L2/3 FrA pyramidal neurons (**Supplementary Fig. 3**)[23]. However, it does not exclude the possibility that BLA inputs could recruit large-scale neuronal networks. Indeed, we found that the *in vivo* photostimulation of BLA neurons with an implanted optical fiber produced large, plateau-like depolarizations in all recorded neurons (peak amplitude: 6.2 ± 1.2 mV*sec; fwhm: 551 ± 80 ms; n=13) (**Fig. 3d**). However, this was observed only when the stimulation was delivered during down-states (**Fig. 3d**), suggesting that BLA inputs might facilitate the transition between down to up-states by recruiting large-scale synaptic networks. Importantly, spontaneous somatic up-states have been suggested to depend on dendritic plateaus[26]. Accordingly, those BLA-mediated plateaus were affected by artificial hyperpolarization that has been shown to efficiently and cell-autonomously block NMDARs *in vivo*[21] (pre: 6.14 ± 1.6 mV*sec, hyper: 3.9 ± 1.5 mV*sec, post: 5.56 ± 1.4 mV*sec; n=4; p=0.004; *anova repeated measures*) (**Fig. 3e, f**).

Given the well-established role of the BLA during the acquisition and expression of learned association[2,3], we next investigated the effect of BLA activation during auditory cue presentation on L2/3 FrA pyramidal neurons (**Fig. 4**). We first verified that *upWGN* alone was able to activate FrA pyramidal neurons in mice chronically implanted with optical fibers. Similarly to the effect of auditory stimulation in non-implanted mice

(see **Fig. 1**), *upWGN* but not *up8kHz* evoked a long-lasting subthreshold depolarization (*upWGN*: 18.8 ± 6.7 mV, n=13; *up8kHz*: -9.7 ± 3 mV, n=8; p=0.01; *Mann-Whitney t-test*). Then, ChR2-expressing BLA neurons were photo-stimulated for 30 s at 0.9 Hz with 27 square light pulses (50 ms), a protocol that precisely mimicked the pattern of auditory stimuli (**Fig. 4a-d**). The coincident photo-activation of BLA[24] during *upWGN* significantly increased the cumulative potential as compared to the presentation of the *upWGN* alone (*upWGN*: 18.8 ± 6.7 mV *vs. upWGN*+light: 39 ± 6.2 mV; n=13; p=0.008; *paired t-test*) (**Fig. 4a, b, e**). Interestingly, the photo-activation of BLA also significantly affected the cumulative potential evoked by *up8kHz* (*up8kHz*: -9.7 ± 3.3 mV *vs. up8kHz*+light: 16.6 ± 3.1 mV; n=8; p<0.001; *paired t-test*) (**Fig. 4c-e**) similarly to the effect of light on *upWGN*-induced cumulative potential (*upWGN*/light: 39 ± 6.2 mV, n=13; *up8kHz*/light: 16.6 ± 3.1 mV, n=8; p=0.138, *Mann-Whitney rank sum test*) (**Fig. 4e**).

Nevertheless, the light-activation of BLA neurons differently altered *upWGN* and *up8kHz*-evoked cumulative potential 30 sec after the end of the stimulation (time point 2). Indeed, we observed that the coincident photo-activation of BLA affected later on-going spontaneous up and down fluctuations following both *upWGN* (*upWGN*: 19.5 ± 7.4 mV *vs. upWGN*/light: 46.4 ± 11.6 mV; n=13; p=0.045; *paired t-test*) (**Fig. 4b**) and *up8kHz* (*up8kHz*: -10.8 ± 5.5 mV *vs. up8kHz*/light: 14.8 ± 6.6 mV; n=8; p=0.013; *paired t-test*) (**Fig. 4d**). However, this long-lasting cooperative effect was significantly higher with Gaussian tone as compared to pure-frequency tone (*upWGN*/light: 46.4 ± 11.6 mV, n=13; *up8kHz*/light: 14.8 ± 6.6 mV, n=8; p=0.039, *Mann-Whitney rank sum test*) (**Fig. 4e**). We also observed that the ectopic application of dAP5 (1mM) to the cortical surface blocked the effect of BLA activation during *upWGN* (light/*upWGN*: 39 ± 6.2 mV, n=13; light/*upWGN*/+dAP5: -26.6 ± 6.7 mV, n=7; p<0.001; *t-test*) (**Fig. 4f**). In fact, this resulted in a negative net effect of light (control: 20.2 ± 6.4 mV; n=13; +dAP5: -30.1 ± 7 mV; n=7) (**Fig. 4g**) that uncovered the activation of feed-forward inhibitory circuits. Thus, it seems that the coordinated activation BLA and auditory inputs generated a highly non-linear depolarization in FrA dendrites that is necessary to overcome evoked inhibition, and eventually induced a long-term alteration of FrA neuronal membrane potential.

## Discriminative learning depends on the activation of BLA-to-FrA circuits

We next questioned the functions of BLA-to-FrA axons during fear learning. It is now well established that the BLA and its prefrontal projections actively acquire signals

about safety[3,7–9,27]. Whether direct BLA-to-FrA axons are also necessary to encode CS- remains unknown. We addressed this question by silencing specifically BLA-to-FrA axons during conditioning but only throughout the presentation of the CS- (**Fig. 5a**). For that, mice were injected bilaterally with a retrograde Cav-2-CMV-Cre[28] into the FrAs together with either AAV9-flex-CBA-ArchT-GFP (ArchT-expressing mice, n=11) or AAV9-CAG-flex-eGFP (control GFP-expressing mice, n=13) into both BLAs (**Fig. 5a**). This resulted in the expression of the light-driven inhibitory proton pump ArchT (or GFP) in a target-specific fraction of BLA neurons that project to the FrA (**Fig. 5b, c**).

Fear learning was then induced by using a discriminative conditioning protocol during which five auditory stimuli (each consisting of 27 pure-tone or WGN pips, 50 ms, 0.9 Hz for 30 s) were positively (CS+) or negatively (CS-) paired with the delivery of a mild electrical shock (0.6 mA) to the paws in a pseudorandom order (**Supplementary Fig. 4a**). Learning was tested 24h later during recall and quantified by multiplying the freezing level in each condition by the corresponding index of discrimination (learning index) (**Fig. 5e**). As expected, control GFP-expressing mice presented robust fear learning (43 ± 5 %; n=13). In contrast, ArchT-expressing mice showed strongly attenuated fear responses during recall (18 ± 3 %; n=11) (**Fig. 5e**), with a learning index that was significantly lower during recall than the one measured in GFP-expressing mice (GFP: 43 ± 5 %, n=13; ArchT: 18 ± 3 %, n=11; $p<0.001$, *t-test*) (**Fig. 5f**). This alteration of fear learning in ArchT-expressing mice resulted from decreased discriminative performance during recall (GFP, 0.8 ± 0.03, n=13; ArchT, 0.56 ± 0.08, n=11; p=0.003, *Kolmogorov-Smirnov test*; p=0.016, *Mann-Whitney rank sum test*) (**Fig. 5g**).

However, the auditory tones (8 kHz and WGN) used for CS+ and CS- during conditioning were counterbalanced across mice (protocol 1: CS+/CS- = 8kHz/WGN respectively; protocol 2: CS+/CS- = WGN/8kHz respectively) (**Supplementary Fig. 4b**). Because WGN appeared more effective in producing dendritic plateau potentials in FrA as compared to pure tone (**Fig. 1 and Fig. 2**), it remains thus possible that fear learning depends on the physical property of the sensory cue that was negatively paired to the footshock[29,30]. Therefore, we analyzed the impact of BLA-to-FrA inactivation on freezing behaviors for each counter-balanced protocol (**Fig. 5h-j and Supplementary Fig. 4c, d**). We found that the time-locked suppression of BLA-to-FrA communication during negatively-paired (*np*) *WGN* (CS-, protocol 1) significantly increased freezing responses upon subsequent *npWGN* presentations (GFP: 5.3 ± 1 %, n=8; ArchT: 13.7 ± 4 %,

n=7;p=0.040, *Mann-Whitney rank sum test*), indicating that CS- acquires safety properties through the activation of a specific population of BLA neurons. Surprisingly, it also decreased freezing behaviors upon positively-paired (*pp) 8kHz* (CS+ protocol 1) (GFP: 55.9 ± 8 %, n=8; ArchT: 34.9 ± 3 %, n=7; p=0.037, *t-test*) (**Fig. 5h**). Consequently, the index of discrimination was strongly attenuated as compared to controls (GFP: 0.8 ± 0.03, n=8; ArchT: 0.49 ± 0.12, n=7; p=0.024, *Mann-Whitney rank sum test*; p=0.04, *Kolmogorov-Smirnov test*) (**Fig. 5j**). In contrast, blocking the activity of BLA-to-FrA axons during protocol 2 failed to affect discriminative performance (GFP: 0.78 ± 0.06, n=5; ArchT: 0.64 ± 0.12, n=4; p=0.335, *t-test*; p=0.17, *Kolmogorov-Smirnov test*) (**Fig. 5j**), with similar freezing responses between GFP- and ArchT-expressing mice upon subsequent *np8kHz* (CS-; GFP: 7.3 ± 2.5, n=5; ArchT: 9.6 ± 3.5, n=4; p=0.611, *t-test*) and *ppWGN* (CS+; GFP: 49.8 ± 10.2, n=5; ArchT: 32.2 ± 8, n=4; p=0.230, *t-test*) (**Fig. 5i**).

Altogether, our data confirm the sophisticated nature of differential conditioning protocols[1,29], during which auditory tones that were not explicitly paired to the footshock might actively participate in discriminative learning (*i.e.* threat *vs.* safety encoding) through the interaction between the BLA and the FrA during conditioning. Importantly, it reveals that the BLA-to-FrA circuit encodes WGN as a safety predictor more efficiently than pure frequency tones.

## BLA-to-FrA axons are not activated by auditory stimulation but are recruited during fear conditioning

The results above suggest a possible cooperative, *Hebbian*-like frontal mechanism that could theoretically integrate into safety memory traces any complex sensory inputs that are contiguous to the activation of BLA-to-FrA axons[14,24,25,31]. Consequently, this mechanism could only occur if BLA-to-FrA axons are activated during conditioning upon CS- presentation. To test this hypothesis, we injected a virus expressing the genetically-encoded calcium indicator GCaMP6f into the right BLA and imaged axonal $Ca^{2+}$ responses in superficial L1 of the right FrA of awake head-restrained mice during fear conditioning (**Fig. 6a-c**). We choose to use exclusively the protocol 1 (**Supplementary Fig. 4b**) as BLA-to-FrA axons appeared to specifically encode safety only when WGN is used as CS- during conditioning (**Fig. 5h-j**).

We conditioned awake mice (n=7) under the 2-photon microscope, during which GCaMP6f calcium transients ($\Delta F/F_0$) provided a direct measure of the activation of BLA

neurons projecting to the FrA (**Fig. 6c-f**). Again, learning was tested 24h later and quantified by assessing the learning index (**Fig. 6d**). Mice were classified as learners (learning+) when the learning index was higher than 20% during recall (**Fig. 6d**). We then compared the activity of individual boutons between mice that learned (learning+, n=4 mice) and those that failed to learn (learning-, n=3 mice). While the activity of 299 individual BLA boutons in FrA was relatively low at rest, it increased significantly upon successive pairings (**Fig. 6e, f**). However, this occurred only for mice that learned (learning+, baseline: 206 events; pairings: 310 events; n=4; +95 ± 51 %; learning-, baseline: 160 events; pairings: 127 events; n=4; -30 ± 10 %; $\chi^2$=18.6, p<0.001). Interestingly, it also never occurred before the end of the first US presentation. Indeed, the number of axonal transients observed during the first CS+ (that is, before the delivery of the first footshock) was not different from baseline (learning+, baseline: 206 events; CS+1/No US: 220 events; n=4; learning-, baseline: 160 events; CS+1/No US: 127 events; n=3; $\chi^2$=3.03, p=0.08) (**Fig. 6g**). In contrast, the activity of boutons measured during both the first CS- (learning+, baseline: 206 events; CS-1/US: 342 events; n=4; learning-, baseline: 160 events; CS-1/US: 129 events; n=3; $\chi^2$=28.9, p<0.001) and the second CS+ (learning+, baseline: 206 events; CS+2/US: 357 events; n=4; learning-, baseline: 160 events; CS+2/US: 126 events; n=3; $\chi^2$=24.3, p<0.001) were significantly increased as compared to the baseline period (**Fig. 6g, h**). Hence, neither the tone alone nor the footshock appeared to have an effect on the activity of BLA-to-FrA axons (**Fig. 6i**). Instead, our data support the idea that BLA axons projecting to the FrA conveyed information about the learning, *i.e.* the CS+/US association itself rather than about the nature or the valence of the auditory tones[14].

## Fear learning occludes auditory tone-specific dendritic plateau potentials

Finally, we tested the impact of fear learning on auditory-evoked dendritic nonlinearities. We observed that plateau potentials evoked by *WGN* were strongly and specifically affected in conditioned animals (**Fig. 7**). Indeed, as compared to naive mice, *WGN* failed to activate FrA pyramidal neurons in conditioned mice (*npWGN*: 5.4 ± 9 mV, n=8; *upWGN*: 27.6 ± 4 mV, n=22; p=0.008) (**Fig. 7a-d**). Thus, the difference between *upWGN* and *up8 kHz*-induced non-linear depolarizations observed in naive mice (14 naive mice; *upWGN*: 27.6 ± 4 mV; *up8kHz*: 1.1 ± 4 mV; n=22; p<0.001; *paired t-test*) disappeared after fear conditioning (5 conditioned mice; *npWGN*: 5.4 ± 9 mV; *pp8kHz*:

0.5 ± 5 mV; n=8; p=0.698; *paired t-test*) (**Fig. 7d**). Accordingly, the averaged number of local dendritic events per dendrite observed upon *npWGN* presentation in awake mice significantly decreased after fear learning (*upWGN*: 3.37 ± 0.3, n=9 naive mice; *npWGN*: 1.88 ± 0.3, n=5 mice; p=0.003) (**Fig. 7e**), indicating that *npWGN* no longer generated local dendritic activation during both anesthesia and wakefulness. We next plotted the tone-evoked cPSP as a function of the behavioral performance (**Fig. 7f**). As opposed to *pp8kHz*-cPSPs that were not different between behavioral performance ($r^2$<0.001), *npWGN* induced stronger plateau depolarizations in low freezing mice indicating that WGN-dendritic plateaus are negatively correlated with behavioral performance (*npWGN*: $r^2$=0.55; *pp8kHz*: $r^2$<0.001) (**Fig. 7f**). Importantly, it indicates that learning occluded multiple input-specific synapses depending on the strength of learning[13], possibly through postsynaptic plasticity mechanisms[32,33].

## DISCUSSION

The present study describes the role of the BLA-to-FrA circuit in the integration of sensory information, and how such process participates in the acquisition of specific memory traces during differential conditioning. We identified segregated auditory and BLA inputs streams whose interaction at the dendritic level of FrA pyramidal neurons might support the creation of safety representation and further influences the representation of cue predicting threat. Although our results depend on the specific association between pure and Gaussian auditory tones during conditioning, they bring new conceptual perspectives to central questions regarding how frontal circuits contribute to learning, thus expanding beyond the BLA-mPFC interactions classically described in fear learning studies[3].

Accumulating evidence from anatomical and functional studies has demontrated that despite its pivotal role in the acquisition and expression of associations between sensory stimuli and the emotional valence of these stimuli[34,35], the mPFC is not directly involved in sensory processing[12,19,36]. In contrast, due to its anatomical connections with distributed cortical and subcortical regions[12,19], the FrA might serve as a hub that coordinates incoming sensory information before reaching the mPFC. Here, we provide the first demonstration, to our knowledge, that auditory sensory stimulation produces dendritic non-linear NMDARs-dependent plateau potentials in FrA L2/3 pyramidal neurons during both anesthesia and wakefulness. More specifically, we observed that the occurrence of these events within the same dendritic branch was higher upon broadband complex noise as compared to pure frequency auditory stimulation (**Fig. 1 and Fig. 2**). Although we cannot exclude that *WGN* tones are structured and further abstracted along the entire auditory system[37], the simplest explanation suggests a wide and heterogeneous distribution of frequency-tuned spines throughout the same FrA dendrite, similar to what has been detailed in the auditory cortex of anesthetized mice[38]. As a consequence, the multiple frequencies composing *WGN* would promote the activation of a dense pattern of neighboring spines that might in turn facilitate the generation and propagation towards the soma of local non-linear events[26]. However, multiple calcium transients occurring simultaneously in multiple dendritic branches are necessary to affect somatic voltage[22]. These data support the idea that, in our study too, *WGN*-induced long-lasting depolarization recorded at the soma (**Fig. 1**) built on multiple local calcium events across multiple dendritic branches. In contrast, pure-frequency

tone appeared unable to activate enough branches simultaneously (**Fig. 2**), thereby making the alteration of somatic voltage less probable (**Fig. 1**).

The FrA and the BLA are anatomically interconnected[13,14,18]. Yet, the functional properties of these connections remain unknown. Our results confirmed that the BLA projected heavily to the superficial layer of the FrA, thereby most likely contacting dendrites of L2/3 pyramidal neurons (**Fig. 3**). The photo-stimulation of ChR2-expressing BLA neurons produced plateau-like depolarizations that were strongly affected by hyperpolarization indicating that they also possibly emerge from dendritic NMDARs-mediated conductances[21]. These BLA-mediated depolarizations were rather weak (**Fig. 3**), but might summate during rhythmic activation to create favorable conditions for the integration of coincident sensory-driven inputs[21,26,39,40]. Alternatively, it is possible that the modest activation of BLA synapses in FrA apical dendrites facilitates or gates the propagation towards the soma of tone-evoked dendritic events[41]. In agreement, we observed that the temporal coincident activation of BLA-to-FrA inputs increased both WGN and 8 kHz-evoked depolarization during anesthesia (**Fig. 4**). Nevertheless, it is striking that only WGN, but not pure-frequency tone, potentiated FrA pyramidal neurons when combined with the photo-stimulation of BLA-to-FrA inputs (**Fig. 4**). Even though this effect was measured no longer than 30 sec after the end of the auditory stimulation, it prompts the speculation that long-range BLA projections in superficial layer of FrA produce additional non-linear dendritic depolarization and gain control over coincident *WGN*-related inputs. Indeed, compelling experimental evidence has demonstrated that non-linear interactions between compartmentalized streams of neural activity induce long-lasting change in synaptic strength and intrinsic excitability[21,25,39,41–43] that could have affected permanently the dynamics of FrA membrane potential.

The BLA presumably transfers to the FrA information that is relevant to fear learning[13,14]. Here, we showed that BLA neurons projecting to the FrA participated in the acquisition of safety memory traces (**Fig. 5e-g**). These data are consistent with recent studies showing an increase of theta synchronization between mPFC and BLA during safety and CS discrimination that possibly inhibits fear response and anxiety-related behaviors[7,8]. However, this occurred only when WGN, but not pure-frequency tone, is used as CS- during conditioning (protocol 1) (**Fig. 5h-j**), thereby revealing for the first time the unique nature of Gaussian tones during learning. In addition, blocking

transiently the activity of BLA projecting neurons during CS- surprisingly altered the expression of fear responses (**Fig. 5**). This is unlikely to be the consequence of a non-sufficient activation of BLA. Instead, given the low number of BLA neurons expressing ArchT (**Fig. 5c**) and their time-locked inhibition during CS- (**Fig. 5a**), we propose alternatively that *npWGN* when combined with the activation of BLA projecting axons might actively influence the representation within the FrA of sensory cues predicting threat (i.e. *pp8kHz*)[1]. Importantly, this hypothesis is supported by the late modification of membrane potential fluctuations observed after the activation of BLA with *WGN* presentation, which occurred at the time when *pp8kHz* is presented during conditioning (**Fig. 4e**).

BLA neurons send projections to multiple cortical and subcortical areas that have been shown to project also to the FrA. Thus it remains possible that the information is transmitted from the BLA to the FrA through indirect pathway[14,44]. Here, we demonstrated that the expression of the genetically encoded calcium indicator GCaMP6 in BLA neurons permitted to monitor optically the activity of target-specific BLA axons during learning (**Fig. 6**). Using this strategy in awake mice, we revealed for the first time that BLA-to-FrA axons were progressively recruited upon successive conditioning trials, thereby ruling out an indirect activation of the FrA circuit. First, we showed that BLA-to-FrA axonal activity was never affected upon the presentation of auditory cues alone (**Fig. 6i**). Our data contrast with previous work showing an increase of local field potential and unit activity in the BLA upon auditory stimulation[45], and suggest instead the existence of a subpopulation of BLA neurons projecting specifically to the FrA that might play specific role during emotional learning. Indeed, those axons were only activated after the first CS+/US pairing, and thus seem to transmit integrated information about the association itself[14]. Nevertheless, the activation of axons was independent of the nature of the CS presented (**Fig. 6g-i**). It appears thus unlikely that BLA-to-FrA axons conveyed the emotional valence of this association. In addition, the activation of BLA alone, while necessary, is not sufficient to trigger learning[24,31]. What might be then the function of its projections during learning? Previous studies highlighted the critical function of the BLA in attention for learning[34,35]. In that context, BLA neurons might signal to frontal circuits any new association independently of its valence, which might be subsequently assigned by the mPFC depending on the nature of the incoming stimuli to further supervise the activity of BLA[3,46].

Collectively, our results raise the possibility that the learned association formed in the BLA could be combined during learning into the FrA with *npWGN*-evoked non-linearities to activate FrA prefrontal neurons. This would eventually lead to the recruitment of neurons into specific cue memory traces. In agreement, we found that differential fear conditioning significantly decreased the number of *npWGN*, but not *pp8kHz*-evoked local dendritic transients (**Fig. 7c-e**). Dendritic plateau potentials have been shown to regulate synaptic strength and synaptic plasticity[21,22,47–49] which might subsequently facilitate the stabilization or pruning of synaptic inputs during learning[50,51]. In support of this view, the level of fear learning has been shown to correlate with the percentage of spine elimination in FrA[13] which possibly explains the negative relation we observed during anesthesia between *npWGN*-evoked subthreshold depolarizations and the strength of learning (**Fig. 7f**).

Taken together, our data revealed for the first time the instructive properties of Gaussian tone during learning, especially when not explicitly paired to the footshock, in encoding safe *vs.* threat predictors. Given that complex tones and WGN are abundant in the environment and communication of most mammals, they might be well-suited to facilitate safety prediction. This is of crucial importance as many anxiety-related disorders such as post-traumatic stress disorder are associated with a loss of cue discrimination that may result in fear generalization to harmless signals[2].

## ACKNOWLEDGEMENTS

We thank Deforges, E. Normand, and B. Darracq (Imetronic) for their technical expertise and support, and A. Holtmaat, P. Fossat, and S. Valerio (AquiNeuro) for their critical reading of our manuscript, and all the members of the Gambino laboratory for technical assistance and helpful discussions. We thank K. Deisseroth and the Standford University, E. Boyden and the MIT, E.J. Kremmer and the IGMM BioCampus Montpellier, L.L. Looger and D. Kim of the GENIE project, and K. Svoboda at the Janelia Farm Research Campus (HHMI) for distributing viral vectors.

This work was supported by the following grants (to FG): FP7 Marie-Curie Career Integration grant 631044, ANR JCJC grant 14-CE13-0012-01, University of Bordeaux and Initiative of Excellence (IdEx) senior chair 2014, Fondation NRJ/Institut de France grant 2015, Laboratory of Excellence (LabEx) Brain grant 2015, and the European Research Council grant ERC-StG-2015-677878.

## AUTHOR CONTRIBUTION

MA, EA, VK, NC performed the experiments. YH and CM provided technical assistance. MA and FG conceived the studies and analyzed the data with the help of NC and EA. FG supervised the research and wrote the manuscript with the help from MA, EA and NC.

## DECLARATION OF INTERESTS

The authors declare no competing financial interests.

## REFERENCES


1. Hall, G. in *Stevens' Handbook of Experimental Psychology* (John Wiley & Sons, Inc., 2002). doi:10.1002/0471214426.pas0301
2. LeDoux, J. E. Emotion circuits in the brain. *Annu. Rev. Neurosci.* **23,** 155–184 (2000).
3. Likhtik, E. & Paz, R. Amygdala-prefrontal interactions in (mal)adaptive learning. *Trends Neurosci.* **38,** 158–166 (2015).
4. Rogan, M. T., Leon, K. S., Perez, D. L. & Kandel, E. R. Distinct neural signatures for safety and danger in the amygdala and striatum of the mouse. *Neuron* **46,** 309–20 (2005).
5. Karalis, N. *et al.* 4-Hz oscillations synchronize prefrontal?amygdala circuits during fear behavior. *Nat. Neurosci.* **19,** 605–612 (2016).
6. Dejean, C. *et al.* Prefrontal neuronal assemblies temporally control fear behaviour. *Nature* **535,** 420–424 (2016).
7. Likhtik, E., Stujenske, J. M., Topiwala, M. A., Harris, A. Z. & Gordon, J. A. Prefrontal entrainment of amygdala activity signals safety in learned fear and innate anxiety. *Nat. Neurosci.* **17,** 106–13 (2014).
8. Stujenske, J. M., Likhtik, E., Topiwala, M. A. & Gordon, J. A. Fear and Safety Engage Competing Patterns of Theta-Gamma Coupling in the Basolateral Amygdala. *Neuron* **83,** 919–933 (2014).
9. Senn, V. *et al.* Long-range connectivity defines behavioral specificity of amygdala neurons. *Neuron* **81,** 428–37 (2014).
10. Sierra-Mercado, D., Padilla-Coreano, N. & Quirk, G. J. Dissociable roles of prelimbic and infralimbic cortices, ventral hippocampus, and basolateral amygdala in the expression and extinction of conditioned fear. *Neuropsychopharmacology* **36,** 529–38 (2011).
11. Vidal-Gonzalez, I., Vidal-Gonzalez, B., Rauch, S. L. & Quirk, G. J. Microstimulation reveals opposing influences of prelimbic and infralimbic cortex on the expression of conditioned fear. *Learn. Mem.* **13,** 728–33 (2006).
12. Hoover, W. B. & Vertes, R. P. Anatomical analysis of afferent projections to the medial prefrontal cortex in the rat. *Brain Struct. Funct.* (2007). doi:10.1007/s00429-007-0150-4
13. Lai, C. S. W., Franke, T. F. & Gan, W.-B. Opposite effects of fear conditioning and extinction on dendritic spine remodelling. *Nature* **483,** 87–91 (2012).
14. Nakayama, D. *et al.* Frontal Association Cortex Is Engaged in Stimulus Integration during Associative Learning. *Curr. Biol.* **25,** 117–123 (2015).
15. Sacchetti, B., Baldi, E., Lorenzini, C. A. & Bucherelli, C. Differential contribution of some cortical sites to the formation of memory traces supporting fear conditioning. *Exp. brain Res.* **146,** 223–32 (2002).
16. Uylings, H. B. M., Groenewegen, H. J. & Kolb, B. Do rats have a prefrontal cortex? *Behav. Brain Res.* **146,** 3–17 (2003).
17. Paxinos, G. & Watson, C. *The rat brain in stereotaxic coordinates*. (Elsevier, 2007).
18. Mátyás, F., Lee, J., Shin, H.-S. S. & Acsády, L. The fear circuit of the mouse forebrain: connections between the mediodorsal thalamus, frontal cortices and basolateral amygdala. *Eur. J. Neurosci.* **39,** 1810–23 (2014).
19. Zhang, S. *et al.* Organization of long-range inputs and outputs of frontal cortex for top-down control. *Nat. Neurosci.* **19,** 1733–1742 (2016).
20. Gambino, F. & Holtmaat, A. Spike-timing-dependent potentiation of sensory surround in the somatosensory cortex is facilitated by deprivation-mediated

disinhibition. *Neuron* **75,** 490–502 (2012).
21. Gambino, F. *et al.* Sensory-evoked LTP driven by dendritic plateau potentials in vivo. *Nature* **515,** (2014).
22. Palmer, L. M. *et al.* NMDA spikes enhance action potential generation during sensory input. *Nat. Neurosci.* **17,** 383–390 (2014).
23. Klavir, O., Prigge, M., Sarel, A., Paz, R. & Yizhar, O. Manipulating fear associations via optogenetic modulation of amygdala inputs to prefrontal cortex. *Nat. Neurosci.* **20,** 836–844 (2017).
24. Johansen, J. P. *et al.* Optical activation of lateral amygdala pyramidal cells instructs associative fear learning. *Proc. Natl. Acad. Sci.* **107,** 12692–12697 (2010).
25. Larkum, M. A cellular mechanism for cortical associations: an organizing principle for the cerebral cortex. *Trends Neurosci.* **36,** 141–51 (2013).
26. Antic, S. D., Zhou, W.-L., Moore, A. R., Short, S. M. & Ikonomu, K. D. The decade of the dendritic NMDA spike. *J. Neurosci. Res.* **88,** 2991–3001 (2010).
27. Sangha, S., Chadick, J. Z. & Janak, P. H. Safety Encoding in the Basal Amygdala. *J. Neurosci.* **33,** 3744–3751 (2013).
28. Hnasko, T. S. *et al.* Cre recombinase-mediated restoration of nigrostriatal dopamine in dopamine-deficient mice reverses hypophagia and bradykinesia. *Proc. Natl. Acad. Sci. U. S. A.* **103,** 8858–63 (2006).
29. Grosso, A., Cambiaghi, M., Concina, G., Sacco, T. & Sacchetti, B. Auditory cortex involvement in emotional learning and memory. *Neuroscience* **299,** 45–55 (2015).
30. Park, S. *et al.* Sound tuning of amygdala plasticity in auditory fear conditioning. *Sci. Rep.* **6,** 31069 (2016).
31. Johansen, J. P. *et al.* Hebbian and neuromodulatory mechanisms interact to trigger associative memory formation. *Proc. Natl. Acad. Sci.* **111,** E5584–E5592 (2014).
32. Rioult-Pedotti, M. S., Friedman, D. & Donoghue, J. P. Learning-induced LTP in neocortex. *Science* **290,** 533–6 (2000).
33. Basu, J. *et al.* Gating of hippocampal activity, plasticity, and memory by entorhinal cortex long-range inhibition. *Science (80-. ).* **351,** aaa5694-aaa5694 (2016).
34. Laviolette, S. R., Lipski, W. J. & Grace, A. A. A subpopulation of neurons in the medial prefrontal cortex encodes emotional learning with burst and frequency codes through a dopamine D4 receptor-dependent basolateral amygdala input. *J. Neurosci.* **25,** 6066–75 (2005).
35. Roesch, M. R., Calu, D. J., Esber, G. R. & Schoenbaum, G. Neural correlates of variations in event processing during learning in basolateral amygdala. *J. Neurosci.* **30,** 2464–71 (2010).
36. Martin-Cortecero, J. & Nuñez, A. Sensory responses in the medial prefrontal cortex of anesthetized rats. Implications for sensory processing. *Neuroscience* **339,** 109–123 (2016).
37. Deneux, T., Kempf, A., Daret, A., Ponsot, E. & Bathellier, B. Temporal asymmetries in auditory coding and perception reflect multi-layered nonlinearities. *Nat. Commun.* **7,** 12682 (2016).
38. Chen, X., Leischner, U., Rochefort, N. L., Nelken, I. & Konnerth, A. Functional mapping of single spines in cortical neurons in vivo. *Nature* **475,** 501–505 (2011).
39. Xu, N. *et al.* Nonlinear dendritic integration of sensory and motor input during an active sensing task. *Nature* **492,** 247–51 (2012).
40. Brandalise, F., Carta, S., Helmchen, F., Lisman, J. & Gerber, U. Dendritic NMDA spikes are necessary for timing-dependent associative LTP in CA3 pyramidal cells. *Nat. Commun.* **7,** 13480 (2016).

41. Jarsky, T., Roxin, A., Kath, W. L. & Spruston, N. Conditional dendritic spike propagation following distal synaptic activation of hippocampal CA1 pyramidal neurons. *Nat. Neurosci.* **8,** 1667–1676 (2005).
42. McGaugh, J. L. Making lasting memories: remembering the significant. *Proc. Natl. Acad. Sci. U. S. A.* **110 Suppl 2,** 10402–7 (2013).
43. Dudman, J. T., Tsay, D. & Siegelbaum, S. A. A role for synaptic inputs at distal dendrites: instructive signals for hippocampal long-term plasticity. *Neuron* **56,** 866–79 (2007).
44. Price, J. L. Comparative aspects of amygdala connectivity. *Ann. N. Y. Acad. Sci.* **985,** 50–8 (2003).
45. Collins, D. R. & Paré, D. Differential fear conditioning induces reciprocal changes in the sensory responses of lateral amygdala neurons to the CS(+) and CS(-). *Learn. Mem.* **7,** 97–103 (2000).
46. Klavir, O., Genud-Gabai, R. & Paz, R. Functional connectivity between amygdala and cingulate cortex for adaptive aversive learning. *Neuron* **80,** 1290–300 (2013).
47. Du, K. *et al.* Cell-type-specific inhibition of the dendritic plateau potential in striatal spiny projection neurons. *Proc. Natl. Acad. Sci. U. S. A.* 201704893 (2017). doi:10.1073/pnas.1704893114
48. Humeau, Y. & Lüthi, A. Dendritic calcium spikes induce bi-directional synaptic plasticity in the lateral amygdala. *Neuropharmacology* **52,** 234–243 (2007).
49. Cichon, J. & Gan, W.-B. Branch-specific dendritic Ca(2+) spikes cause persistent synaptic plasticity. *Nature* **520,** 180–5 (2015).
50. Holtmaat, A. & Caroni, P. Functional and structural underpinnings of neuronal assembly formation in learning. *Nat. Neurosci.* **19,** 1553–1562 (2016).
51. Li, W., Ma, L., Yang, G. & Gan, W.-B. REM sleep selectively prunes and maintains new synapses in development and learning. *Nat. Neurosci.* **20,** 427–437 (2017).

## METHODS

All experiments were performed in accordance with the Guide for the Care and Use of Laboratory Animals (National Research Council Committee (2011): Guide for the Care and Use of Laboratory Animals, 8th ed. Washington, DC: The National Academic Press.) and the European Communities Council Directive of September 22th 2010 (2010/63/EU, 74). Experimental protocols were approved by the institutional ethical committee guidelines for animal research (N°50DIR_15-A) and by the French Ministry of Research (N°02169.01). We used male C57Bl6/J 6-weeks old mice from Charles River that were housed with littermates (3-4 mice per cage) in a 12-h light-dark cycle. Cages were enriched and food and water were provided *ad libitum*.

### Surgery and virus injection

Mice were anesthetized with an intraperitoneal (i.p.) injection of a mix containing medetomidine (sededorm, 0.27 mg $kg^{-1}$), midazolam (5 mg $kg^{-1}$) and fentanyl (0.05 mg $kg^{-1}$) in sterile NaCl 0.9% (MMF-mix). Analgesia was achieved by local application of 100 µl of lidocaine (lurocaine, 1%) and subcutaneous (s.c.) injection of buprenorphine (buprécare, 0.05 mg $kg^{-1}$). 40 µl of dexamethasone (dexadreson, 0.1mg $ml^{-1}$) was administrated intramuscularly (i.m.) in the quadriceps to prevent inflammation potentially caused by the friction of the drilling. A heating-pad was positioned underneath the animal to keep the body temperature at 37ºC. Eye dehydration was prevented by topical application of ophthalmic gel. The skin above the skull was disinfected with modified ethanol 70% and betadine before an incision was made. Stereotaxic injections were done as previously described[21] . Briefly, the bregma and lambda were aligned (x and z) and a hole for injection was made using a pneumatic dental drill (BienAir Medical Technologies, AP-S001). The injections were targeted either to the layer 2/3 of the FrA (from bregma: AP, +2.8 mm; DV, -0.2-0.3 mm; ML ±1.0 mm) or to the BLA (from bregma: AP, -1.3 mm; DV, -4.5 to 4.8 mm; ML, ±2.9 mm), or to both at the same time. 200 nl of virus were injected at a maximum rate of 60 nl/min, using a glass pipette (Wiretrol, Drummond) attached to an oil hydraulic manipulator (MO-10, Narishige).

The following viruses were used depending on the experiments. AAV-ChR2 (AAV9.CamKIIa.hChR2(H134R).eYFP.WPRW.SV40, Penn Vector Core) was unilaterally injected in the right BLA, whereas AAV-ArchT-Flex (AAV9.CBA.flex.Arch-

GFP.WPRE.SV40, Penn Vector Core) and CAV2-Cre (Cav2.CMV.Cre, IGMM BioCampus Montpellier) were bilaterally injected into the BLA and FrA, respectively. Control experiments were performed using an AAV containing the DNA construct for GFP (AAV9.CAG.flex.eGFP.WPRE.bGH). For axonal calcium imaging, AAV-GCaMP6f (AAV1.Syn.GCaMP6f.WPRE.SV40, Penn Vector Core) was injected to the right BLA. For dendritic calcium imaging, AAV-GCaMP6s (AAV9.Syn.Flex.GCaMP6s.WPRE.SV40, Penn Vector Core) and a 1:10000 dilution of AAV-Cre (AAV1.hSyn.Cre.WPRE.hGH, Penn Vector Core) were injected together into the right FrA. After injections, the viruses were allowed to diffuse for at least 10 min before the pipette was withdrawn. Mice were then either prepared for cranial window implantation or waked-up by a sub-cutaneous injection of a mixture containing atipamezole (revertor, 2.5 mg $kg^{-1}$), flumazenil (0.5 mg $kg^{-1}$), and buprenorphine (buprécare, 0.1 mg kg-1) in sterile NaCl 0.9% (AFB-mix).

The cranial windows were made as previously described[21]. Briefly, after skull's exposure a ~5 mm plastic chamber was attached on the area of interest and a 3 mm craniotomy was made on the right hemisphere above FrA and M2, with a pneumatic dental drill, leaving the dura intact. The craniotomy was covered with sterile saline (0.9% NaCl) and sealed with a 3 mm glass cover slip after viral injection (for imaging experiments). The chamber, the cover slip and a custom-made stainless steel head stage were well attached to the skull using dental acrylic and dental cement (Jet Repair Acrylic, Lang Dental Manufacturing).

To evaluate the viral expression profiles in BLA and FrA, fixed brain slices were imaged post-hoc using a wide-field epifluorescence microscope (Nikon, Eclipse N-iU). Illumination was set such that the full dynamic range of the 16-bit images was utilized. A two-dimensional graph of the intensities of pixel was plot using Fiji Software. 16-bit images' brightness was processed and masks were registered to the corresponding coronal plates (ranging from -1.94 to -2.70 mm) of the mouse brain atlas using Illustrator (Adobe), at various distances anterior (FrA) or posterior (BLA) to the bregma.

**Fear conditioning and quantification of learning**

At least 5 days before starting behavioral experiments, mice went through handling with the same experimenter that performed the experiments in order to decrease stress. For consistency across experiments, mice were then habituated to auditory tones during 3 successive days. During habituation, mice were placed on the

conditioning compartment (context A, consisting of a squared box with a grid floor that allows the delivery of a foot shock and with home cage litter under; cleaned between individuals with 70% ethanol). Two conditional auditory stimuli (CS) (8 kHz pure tone; and white Gaussian noise (WGN); each composed of 27 pips, 50 ms in duration, 0.9 Hz for 30 s) were presented 4 times with a 80 dB sound pressure level and variable inter stimulus interval (ISI). The freezing time during each CS presentation was measured and the mice returned to their home cage. Mice were fear conditioned 24 hours after the last habituation phase by using a classical differential protocol. Briefly, mice were exposed to context A and 5 auditory tones (CS+) were paired with the unconditional stimulus (US, 1s foot-shock, 0.6 mA). The onset of US coincided with the CS+ offset. 5 CS- presentations were intermingled with CS+ presentations with a variable (10-60 s) ISI. CS were counterbalanced with WGN and 8 kHz pure tones being used as CS+ and CS-, respectively. Recall tests were carried out 24, 48 and 72 hours after the conditioning phase by measuring the freezing time during the presentation of 2 CS+ and 2 CS- in a new context (context B, consisting of a cylindrical white compartment with home cage litter on the floor; cleaned between individuals with septanios MD 2%).

For optogenetic experiments using *archeorhodopsin* (ArchT) or GFP controls, mice were subjected to the same behavioral protocol described above. Optogenetic inhibition of BLA-to-FrA projections upon CS- presentation was achieved during the conditioning phase by synchronizing each pip (50 ms) composing the CS- with a 50 ms-laser pulse. For the experiments in which the conditioning phase was taken place under the 2 photon microscope, the context consisted of the microscope shading box in which the mice were head-restrained in a custom tube containing a shocking grid at the bottom. CS and US presentations were triggered by a MATLAB routine, associated to a pulse-stimulator (Master-8, A.M.P.I) capable of triggering the foot shock. For somatic and dendritic calcium imaging experiments, behavior was assessed at least 6 hours after imaging sessions. For whole-cell recordings experiments, mice were anesthetized and prepare for patch recordings immediately after behavior.

For each behavioral session, the total time duration (sec) of freezing episodes upon CS+ and CS- presentation was quantified automatically using a fire-wire CCD-camera connected to an automated freezing detection software (AnyMaze, Ugo Basile, Italy), and expressed as % of freezing. Learning index was further quantified for each CS

by multiplying the % of freezing in each condition by the corresponding index of discrimination by using the following equation:

$$learning\ index\ (\%) = freezing\ (\%) \times \frac{freezing\ CS^{+}(\%) - freezing\ CS^{-}(\%)}{freezing\ CS^{+}(\%) + freezing\ CS^{-}(\%)}$$

Learning index <20% during recall was considered as a failure of conditioning.

**In vivo whole cell recordings**

Isoflurane (4% with ~0.5 l $min^{-1}$ $O_2$) combined with an i.p. injection of urethane (1.5 g $kg^{-1}$, in lactated ringer solution containing in [mM] 102 NaCl, 28 Na L Lactate, 4 KCl, 1.5 $CaCl_2$) was used to induce anesthesia and prolonged by supplementary urethane (0.15 g $kg^{-1}$) if necessary. To prevent risks of inflammation, brain swelling and salivary excretions, 40 µl of dexamethasone (dexadreson, 0.1 mg $ml^{-1}$, i.m.) and glycopyrrolate (Robinul-V, 0.01 mg $kg^{-1}$, s.c.) were injected before the surgery. Adequate anesthesia (absence of toe pinch and corneal reflexes, and vibrissae movements) was constantly checked and body temperature was maintained at 37°C using a heating-pad positioned underneath the animal. Ophthalmic gel was applied to prevent eye dehydration. Analgesia was provided as described for viral injection (with lidocaine and buprenorphine). After disinfection of the skin (with modified ethanol 70% and betadine), the skull was exposed and a ~3mm plastic chamber was attached to it above the prefrontal cortex using a combination of super glue (Loctite) and dental acrylic and dental cement (Jet Repair Acrylic, Lang Dental Manufacturing). A small ~1 x 1 mm craniotomy centered above the FrA (+2.8 mm from bregma, ±1.0 mm midline) was made using a pneumatic dental drill, leaving the dura intact.

Whole-cell patch-clamp recordings of L2/3 pyramidal neurons were obtained as previously described [21] Briefly, high-positive pressure (200–300 mbar) was applied to the pipette (5–8 MΩ) to prevent tip occlusion, when passing the pia. Immediately after, the positive pressure was reduced to prevent cortical damage. The pipette resistance was monitored in the conventional voltage clamp configuration during the descendent pathway through the cortex (until -200 µm from the surface) of 1 µm steps. When the pipette resistance abruptly increased, the 3–5 GΩ seal was obtained by decreasing the positive pressure. After break-in, Vm was measured, and dialysis was allowed to occur for at least 5 min before launching the recording protocols. Current-clamp recordings

were made using a potassium-based internal solution (in mM: 135 potassium gluconate, 4 KCl, 10 HEPES, 10 Na2-phosphocreatine, 4 Mg-ATP, 0.3 Na-GTP, and 25 µM, pH adjusted to 7.25 with KOH, 285 mOsM), and acquired using a Multiclamp 700B Amplifier (Molecular Devices). Spontaneous activity was recorded prior, during and after the presentation of auditory stimulation. Spiking pattern of patched cells was analyzed to identify pyramidal neurons. dAP5 (1 mM, Tocris) was topically applied to the dura mater, before whole cell recordings. Offline analysis was performed using custom routines written in Sigmaplot (Systat), IGOR Pro (WaveMetrics) and Matlab (Mathworks).

**In vivo optogenetics**

After virus injection for ChR2 or ArchT expression, mice were subsequently implanted with fiber optic cannula for optogenetics (CFML22U, Thorlabs) in the BLA. The optic fibers were previously cleaved with a fiber optic scribe (S90R, Thorlabs) at 4.5mm for BLA. The cannula were guided and stereotaxically inserted inside the brain with the help of a cannula holder (XCL, Thorlabs) through the same burr hole used for the viral injections (BLA coordinates from bregma: AP, -1.3mm; DV, -4.5 mm; ML, ±2.9mm) and secured in place with a mix of super glue (Loctite) and dental acrylic and dental cement (Jet Repair Acrylic, Lang Dental Manufacturing). Anesthesia was reversed using AFB-mix for mice assigned to behavioral experiments. For *in vivo* photostimulation of ChR2-expressing BLA neurons, the fiber optic cannula and the optogenetic patch cable (M83L01, Thorlabs) were connected through a ceramic split mating sleeve (ADAL1, Thorlabs). The patch cable was then coupled to a blue DPSS laser (SDL-473-050MFL, Shanghai Dream Lasers Technology) which was triggered by a pulse-stimulator (Master-9, A.M.P.I), able to synchronize 50 ms laser pulses with 50 ms sound pips composing the CS. For inhibition of BLA-to-FrA projections during learning, *in vivo* bilateral optic stimulation of ArchT-expressing neurons was achieved by coupling the optic fibers implanted in BLA to a multimode fiber optic coupler (FCMH2-FCL, Thorlabs), with a ceramic split mating sleeve, and subsequently connected to a yellow DPSS laser (SDL-LH-1500, Shanghai Dream Lasers Technology).

764 **In vitro whole-cell recordings**

765 Mice were anesthetized with a mixture of ketamine/xylazine (100mg/kg and
766 10mg/kg respectively) and cardiac-perfused with ice-cold, oxygenated (95% O2, 5%
767 CO2) cutting solution (NMDG) containing (in mM): 93 NMDG, 93 HCl, 2.5 KCl, 1.2
768 NaH2PO4, 30 NaHCO3, 25 Glucose, 10 MgSO4, 0.5 CaCl2, 5 Sodium Ascorbate, 3 Sodium
769 Pyruvate, 2 Thiourea and 12mM N-Acetyl-L-cysteine (pH 7.3-7.4, with osmolarity of
770 300-310 mOsm). Brains were rapidly removed and placed in ice-cold and oxygenated
771 NMDG cutting solution (described above). Coronal slices (300 µm) were prepared using
772 a Vibratome (VT1200S, Leica Microsystems, USA) and transferred to an incubation
773 chamber held at 32°C and containing the same NMDG cutting solution. After this
774 incubation (9-11 min), the slices were maintained at room temperature in oxygenated
775 modified ACSF containing (mM): 92 NaCl, 2.5 KCl, 1.2 NaH2PO4, 30 NaHCO3, 20 HEPES,
776 25 Glucose, 2 MgSO4, 2 CaCl2, 5 Sodium Ascorbate, 3 Sodium Pyruvate, 2 Thiourea and
777 12mM N-Acetyl-L-cysteine (pH 7.3-7.4, with osmolarity of 300-310 mOsm) until
778 recording.

779 Whole-cell recordings of layer 2/3 FrA principal neurons were performed on
780 coronal slices (from bregma: +2.58 mm to +3.08 mm) at 30-32ºC in a superfusing
781 chamber. Patch electrodes (3-5 MΩ) were pulled from borosilicate glass tubing and filled
782 with a K-gluconate-based intracellular solution (in mM: 140 K-gluconate, 5 QX314-Cl, 10
783 HEPES, 10 phosphocreatine, 4 Mg-ATP and 0.3 Na-GTP (pH adjusted to 7.25 with KOH,
784 295 mOsm). BLA-to-FrA monosynaptic EPSCs were elicited by 1-50 ms light
785 stimulations delivered by an ultrahigh power 460 nm LED (Prizmatix Ltd, Israel). Data
786 were recorded with a Multiclamp700B (Molecular Devices, USA), filtered at 2 kHz and
787 digitized at 10 kHz. Data were acquired and analysed with pClamp10.2 (Molecular
788 Devices).

789

790 **2-photon laser-scanning microscope (2PSLM)-based calcium imaging**

791 Head-fixed awake mice were placed and trained under the microscope every day
792 for at least 7 days prior to the experiment, and then imaged 21 to 35 days after virus
793 injection using an *in vivo* non-descanned FemtoSmart 2PLSM (Femtonics, Budapest,
794 Hungary) equipped with a ×16 objective (0.8 NA, Nikon). The MES Software (MES v.4.6;
795 Femtonics, Budapest, Hungary) was used to control the microscope, the acquisition
796 parameters, and the TTL-driven synchronization between the acquisition and

auditory/footshock stimuli. The GCaMPs were excited using a Ti:sapphire laser operating at λ=910 nm (Mai Tai DeepSee, Spectra-Physics) with an average excitation power at the focal point lower than 50 mW. Time-series images were acquired within a field-of-view of 300 x 300 µm (256 lines, 1ms/line) for axons; for dendrite: 200 x 60 µm (64 lines, 0.5ms/line). Each imaging session consisted of 30 s of baseline recording followed by 8 gaussian and 8 pure (8kHz)-tone auditory stimuli delivered with pseudo-random delays. We imaged on average 3500 frames (~900 s) per session, and no visible photo-bleaching was observed. Images were then analyzed as previously described [21] using custom routines written in Fiji and Matlab (Mathworks). We registered images over time and corrected XY motion artifacts within a single imaging session by using cross-correlation based on rigid body translation (Stack aligner, Image J, NIH, USA). Motion corrections were then assessed by computing pair-wise 2D correlation coefficient (Image correlation, Image J, NIH, USA), and frames were discarded from the analysis if lower than 0.7. Similar rigid body translation was used to align inter-sessions images with the session 4 (first session post learning) selected as a reference template. Regions of interest (ROIs) for pyramidal neurons and putative axonal boutons were selected and drawn manually. All pixels within each ROI were first averaged providing a single time-series of raw fluorescence. To limit the effect of fluorescence drift over time, the baseline fluorescence ($F_0$) was calculated as the mean of the lower 50% of previous 3 s fluorescence values. Change in fluorescence ($\Delta F_t/F_0$) was defined as $(F_t-F_0)/F_0$, were $F_t$ is the fluorescence intensity at time $t$ (time of the first pixel in each frame). Calcium events were then detected using a template-based method with a custom library of calcium transients. Templates were created by extracting and averaging segments of data that were visually identified as corresponding to a transient. Calcium transients whose peak amplitude reached a 3 X background standard deviation threshold were further considered for analysis. Each detected event was inspected visually and analysis was restricted to detected events rather than on raw fluorescence. For extracting spatial profiles of dendritic calcium events, small ROIs of 2 X 2 pixels are generated along the dendrite by using custom routine in Fiji. The spread of $Ca^{2+}$ events was then quantified by calculating the full-width at half-max (fwhm, expressed as % of total dendritic length) of the normalized gaussian fit at the time when the averaged $\Delta F/F_0$ was maximal.

## Data availability and Statistics

All data generated or analyzed during this study are included in the manuscript, and provided in the supplementary statistical table. Data are presented as the median ± interquartile range or mean ± sem (except where stated differently). All statistics were performed using Matlab (Mathworks) and Sigmaplot (Systat) with an α significant level set at 0.05. Normality of all value distributions and the equality of variance between different distributions were first assessed by the Shapiro-Wilk and Levene median tests, respectively. Standard parametric tests were only used when data passed the normality and equal variance tests. Non-parametric tests were used otherwise. Only two-sided tests were used. When applicable, pair-wise multiple post-hoc comparisons were done by using the Holm-Sidak method. Randomization and blinding methods were not used. No statistical methods were used to estimate sample size, but β-power values were calculated for parametric tests.

## FIGURES AND LEGENDS

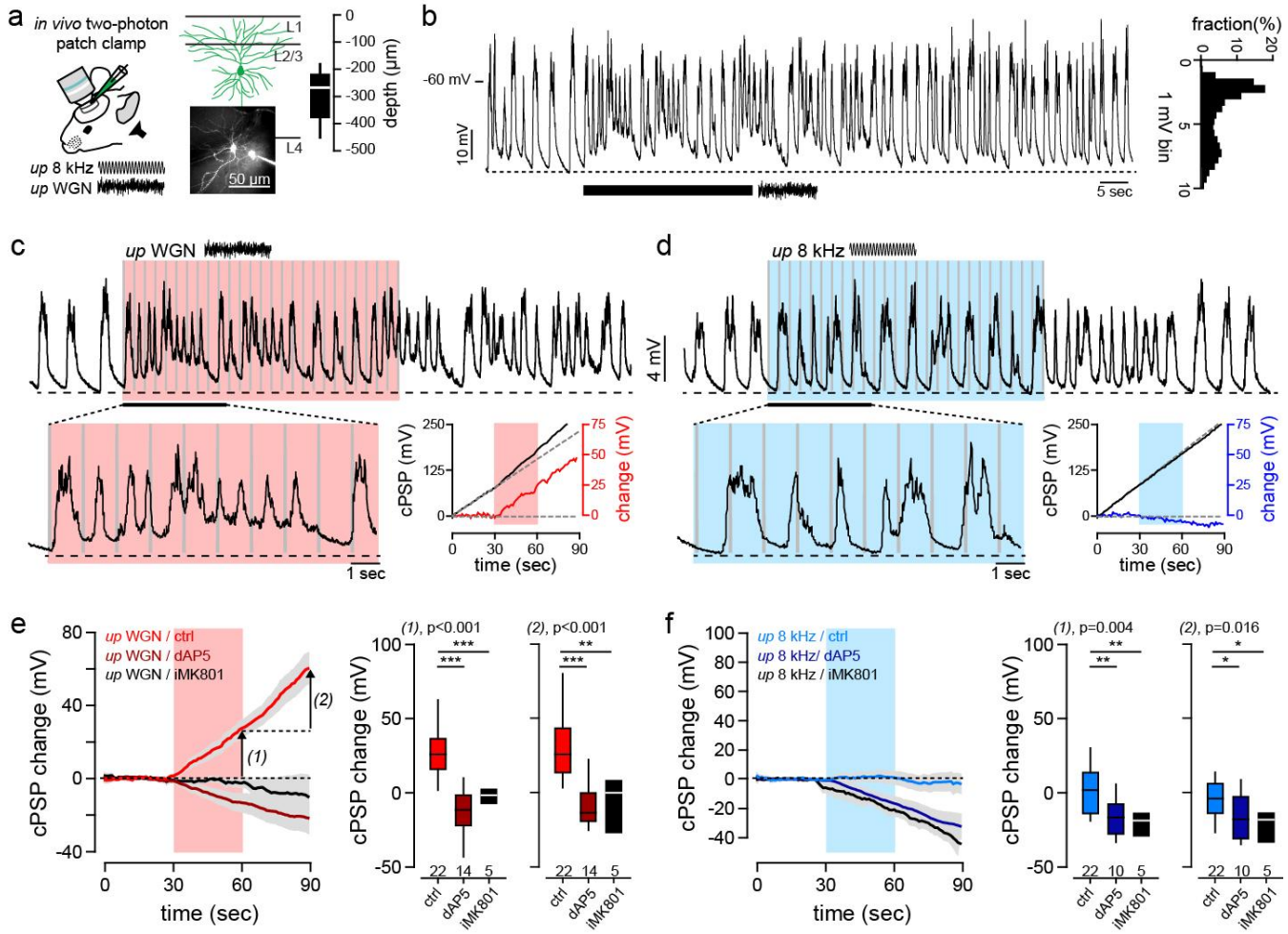


**Fig. 1**

**Figure 1. Gaussian auditory stimulation evokes NMDARs-dependent plateau potentials in FrA pyramidal neurons**

**a,** Auditory-evoked postsynaptic potentials (PSPs) were recorded from L2/3 FrA pyramidal neuron obtained under urethane anesthesia with 2P visual guidance. Depth of recorded cells is indicated.

**b,** Example of recorded FrA neuron showing typical spontaneous slow wave fluctuations. Black bar indicates timing of gaussian stimulation. *Right*, Membrane potential probability histogram.

**c, d,** Example traces of postsynaptic membrane potential recorded from an individual FrA L2/3 pyramidal neuron upon WGN (**c**) and pure 8kHz (**d**) auditory stimulation (gray bars: 27 pips, 50 ms in duration, 0.9 Hz, 30 s). The effect of both stimuli was tested on the same cell. *Bottom right panels,* sensory-evoked PSP changes (red and blue) that were calculated by subtracting the cumulative PSP (cPSP, solid black line) by its linear regression during the baseline period (dashed black line).

**e,** *Left*, Averaged cPSP change (± sem) evoked by WGN, with or without the blockade of NMDARs (dAP5 or iMK801). Auditory stimulation is depicted by the red bar; arrows, analysis time points 1 (end of stimulation) and 2 (30 sec later). *Right*, Effect of dAP5 and iMK801 on cPSPs change at time points 1 (left, $p<0.001$, *one way anova*) and 2 (right, $p<0.001$, *one way anova*). Boxplots represent median and interquartile range (Ctrl, n=22, dAP5, n=14, iMK801, n=5; ***, $p<0.001$, **, $p<0.01$, *Holm-Sidak multiple comparisons*).

**f,** Same representation as (**e**) but for pure 8kHz-evoked cPSP change (Ctrl, n=22, dAP5, n=10, iMK801, n=5; p=0.04 and 0.016, *one way anova*; **, $p<0.01$, *, $p<0.05$, *Holm-Sidak comparisons*).

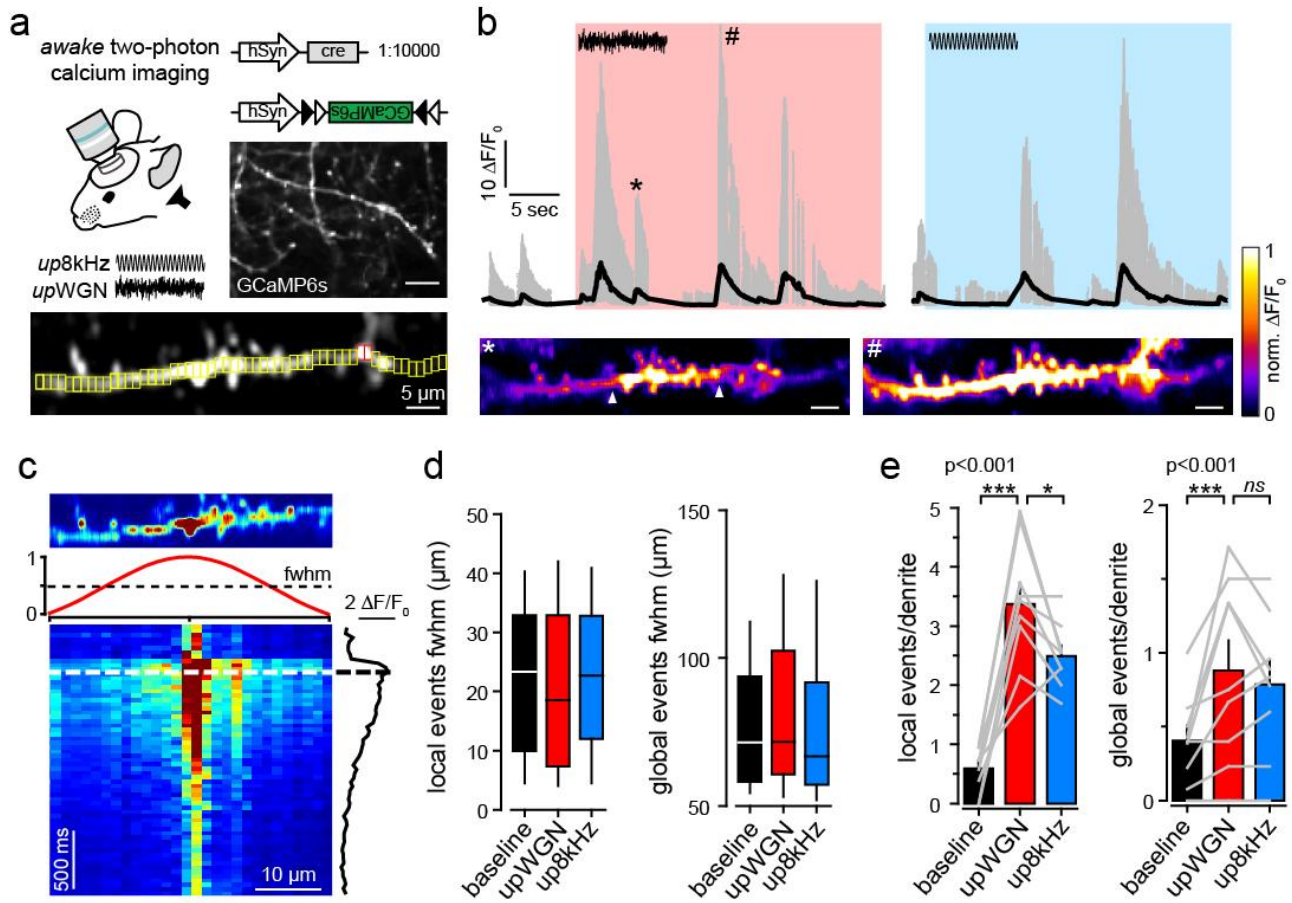


**Fig. 2**

**Figure 2. Auditory-evoked $Ca^{2+}$ events in dendritic tufts of FrA L2/3 pyramidal neurons**

**a,** *Top*, experimental strategy. Mice were double-infected with AAV9-Syn-GcaMP6s-Flex and 1/10000 diluted AAV1-hSyn-Cre viruses resulting in sparse expression of GCaMP6s. Scale bar, 10 µm. $Ca^{2+}$ events in individual dendrites were then imaged in L1 with 2P upon auditory stimulation (*upWGN* and *up8kHz*) in awake mice. *Bottom*, example of GCaMP6s fluorescence standard deviation image with ROIs in yellow. Red ROIs overlapped with another dendrite, and were hence excluded from the analysis.

**b,** *Top*, example of multiple $Ca^{2+}$ transients ($\Delta F/F_0$) recorded in a single dendrite during baseline and upon *upWGN* (red) and *up8kHz* (blue). Grey lines, $\Delta F/F_0$ measured from small ROIs shown in (**a**) (all ROIs superimposed). Black line, mean $\Delta F/F_0$ averaged over all ROIs, respectively. *Bottom*, example of local (*) and global (#) dendritic $Ca^{2+}$ events. Scale bar, 5µm.

**c,** The spread of $Ca^{2+}$ events was quantified by calculating the full-width at half-max (fwhm, dashed line) of the normalized gaussian fit (red) at the time when the averaged $\Delta F/F_0$ was maximal.

**d,** fwhm of local (*left*) and global (*right*) events were pooled together and averaged. Boxplots represent median and interquartile range (n=104 dendritic branches).

**e,** The number of local (left) and global (right) $Ca^{2+}$ events observed during baseline and upon auditory stimulations was averaged over 9 imaged mice ($p<0.001$, *one way repeated measures anova*; *, $p<0.05$, ***, $p<0.001$, *ns*, non-significant, *Holm-Sidak multiple comparisons*). Grey lines represent individual mice.

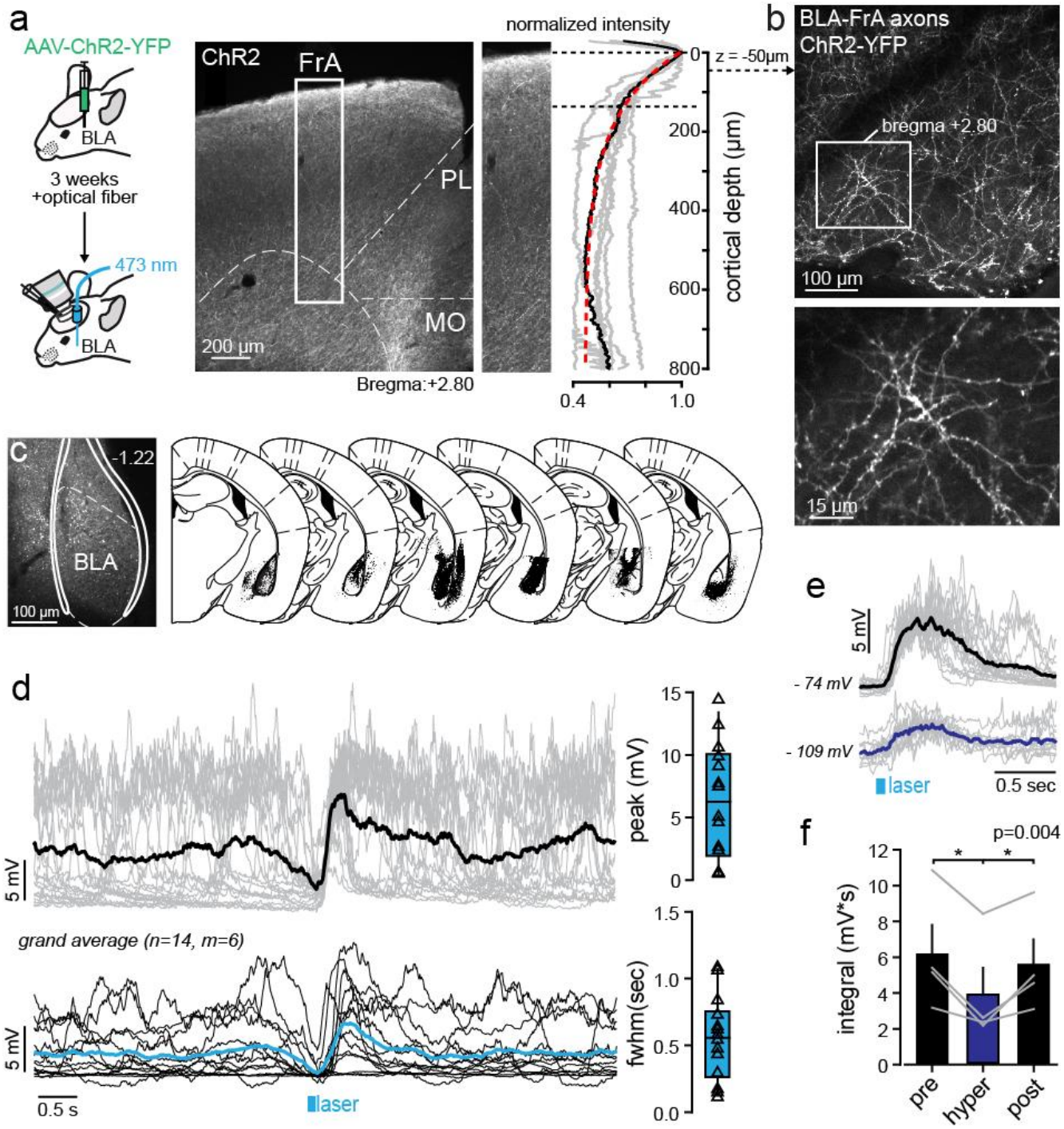


**Fig. 3**

**Figure 3. BLA neurons project to FrA and activate L2/3 pyramidal neurons**

**a,** Experimental strategy. *Left*, BLA neurons were transfected with AAV9-CamKIIa-hChR2-eYFP, and ChR2-expressing BLA neurons were then photo-stimulated *in vivo* with a DPSSL (λ = 473 nm) through a chronically-implanted optical fiber. *Middle*, example of a cortical slice with ChR2-GFP fluorescence in the FrA. *PL, prelimbic cortex; MO, medial orbital cortex*. *Right*, fluorescence intensity profiles measured in the FrA (white box) of 6 different animals in which injections targeted BLA.

**b,** Examples of ChR2-expressing axons imaged in superficial layer 1 with 2P microscopy.

**c,** *Left*, representative example of the ChR2-GFP expression profile in the mouse BLA. *Right*, Coronal diagrams of the brains from 6 mice showing the expression profiles (in black) of ChR2-GFP. Diagrams were adapted from the Paxinos atlas.

**d,** *Top*, single-cell examples of sustained depolarizations in FrA by the photostimulation of BLA neurons. Gray lines, single trials; black line, average of 20 trials. *Bottom*, grand-average (blue) of evoked PSPs from 14 cells (m=6 mice). Blue bar, light duration. *Right*, Peak amplitude (top) and fwhm (bottom) of evoked PSP.

**e,** Single-cell examples of BLA-mediated PSPs at resting membrane potential (top) and upon cell-autonomous hyperpolarization

**f,** BLA-mediated PSP integrals before (pre), during (hyper) and after (post) hyperpolarization (n=4, $p=0.004$, one way repeated measures anova; *, $p<0.01$, Holm-Sidak multiple comparisons).

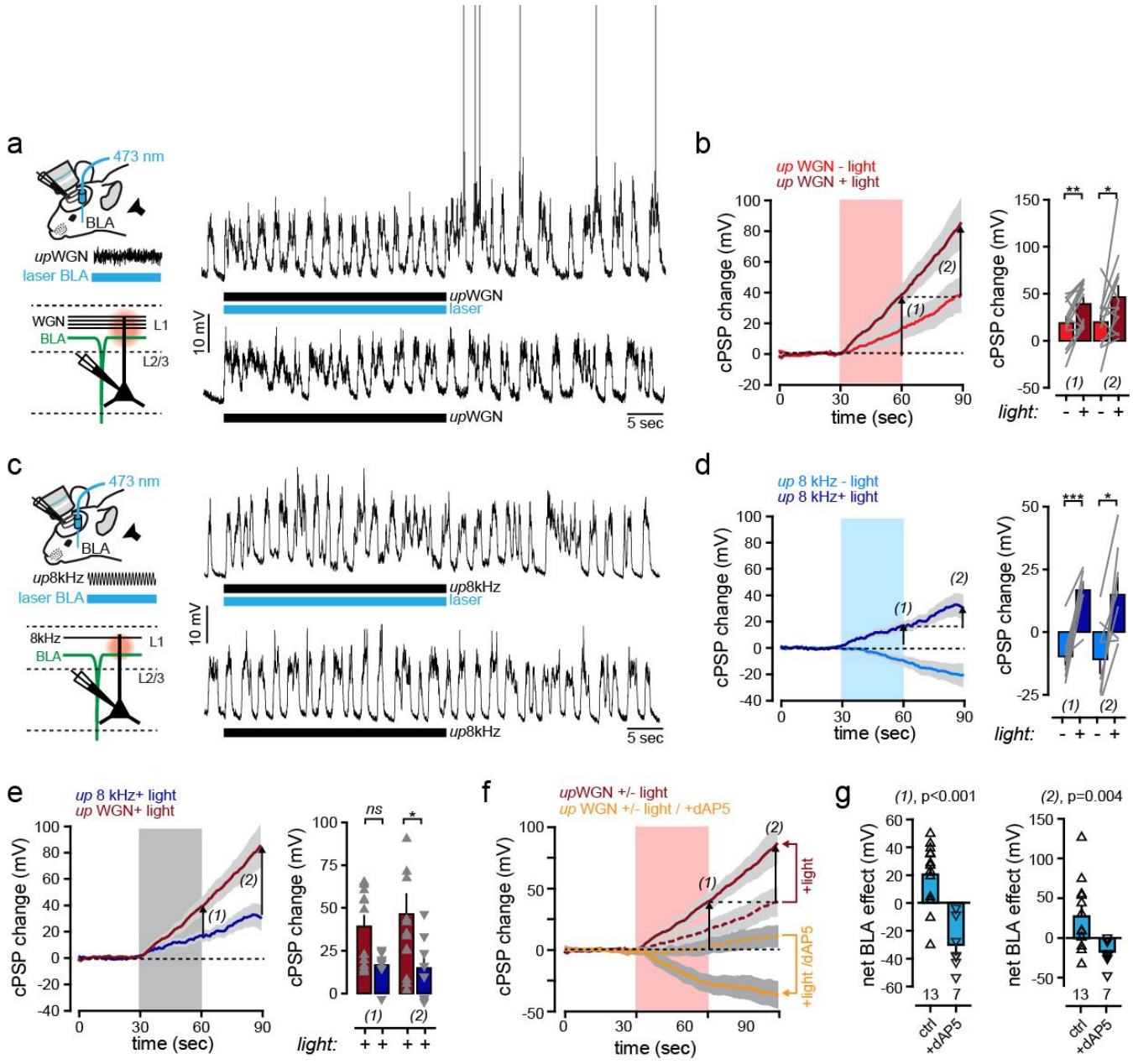


**Fig. 4**

**Figure 4. Coincident activation of BLA excitatory inputs to the FrA reinforces L2/3 pyramidal neurons**

**a,** *Left*, Co-activation protocol. ChR2-expressing BLA neurons were photo-stimulated during WGN auditory stimulation. *Right*, Example of traces of postsynaptic membrane potential recorded from individual FrA L2/3 pyramidal neurons upon WGN paired (*top*) or not (*bottom*) with the photo-stimulation of ChR2-expressing BLA neurons. Black and blue bars below the traces indicate the duration of the stimulation.

**b,** *Left*, Averaged cPSP change (± sem) upon paired (*upWGN* +light) and unpaired (*upWGN* -light) WGN. Arrows, analysis time points 1 (end of stimulation) and 2 (30 sec later). *Right*, Effect of photostimulation on WGN-evoked cPSP (n=13; **, $p<0.01$; *, $p<0.05$; paired t-test). Boxplots represent median and interquartile range, gray lines indicate paired experiments.

**c, d,** Same presentation as in (**a**) and (**b**) but for *up8kHz* (n=8; ***, $p<0.001$; *, $p<0.05$; paired t-test).

**e,** *Left*, Averaged cPSP change (± sem) upon paired *upWGN* (*upWGN* +light) and paired *up8kHz* (*up8kHz* +light). Arrows, analysis time points 1 (end of stimulation) and 2 (30 sec later). *Right*, Effect of photostimulation on *upWGN* (dark red) and *up8kHz* (blue)-evoked cPSP at time points 1 and 2 (*upWGN* +light, n=13; *up8kHz* +light, n=8; *, $p<0.05$, Mann-Whitney rank sum test).

**f,** Averaged cPSP change (± sem) upon paired (solid line) and unpaired (dashed line) WGN, with (yellow) or without (dark red) the blockade of NMDARs (dAP5). Arrows, analysis time points 1 (end of stimulation) and 2 (30 sec later).

**g,** The net BLA effect (in mV) was quantified for each cell (triangle) at time points 1 (left; $p<0.001$, *t-test*) and 2 (right; $p<0.004$, *t-test*) by subtracting cPSP change with photostimulation by the cPSP change before photostimulation. The number of cells is indicated below.

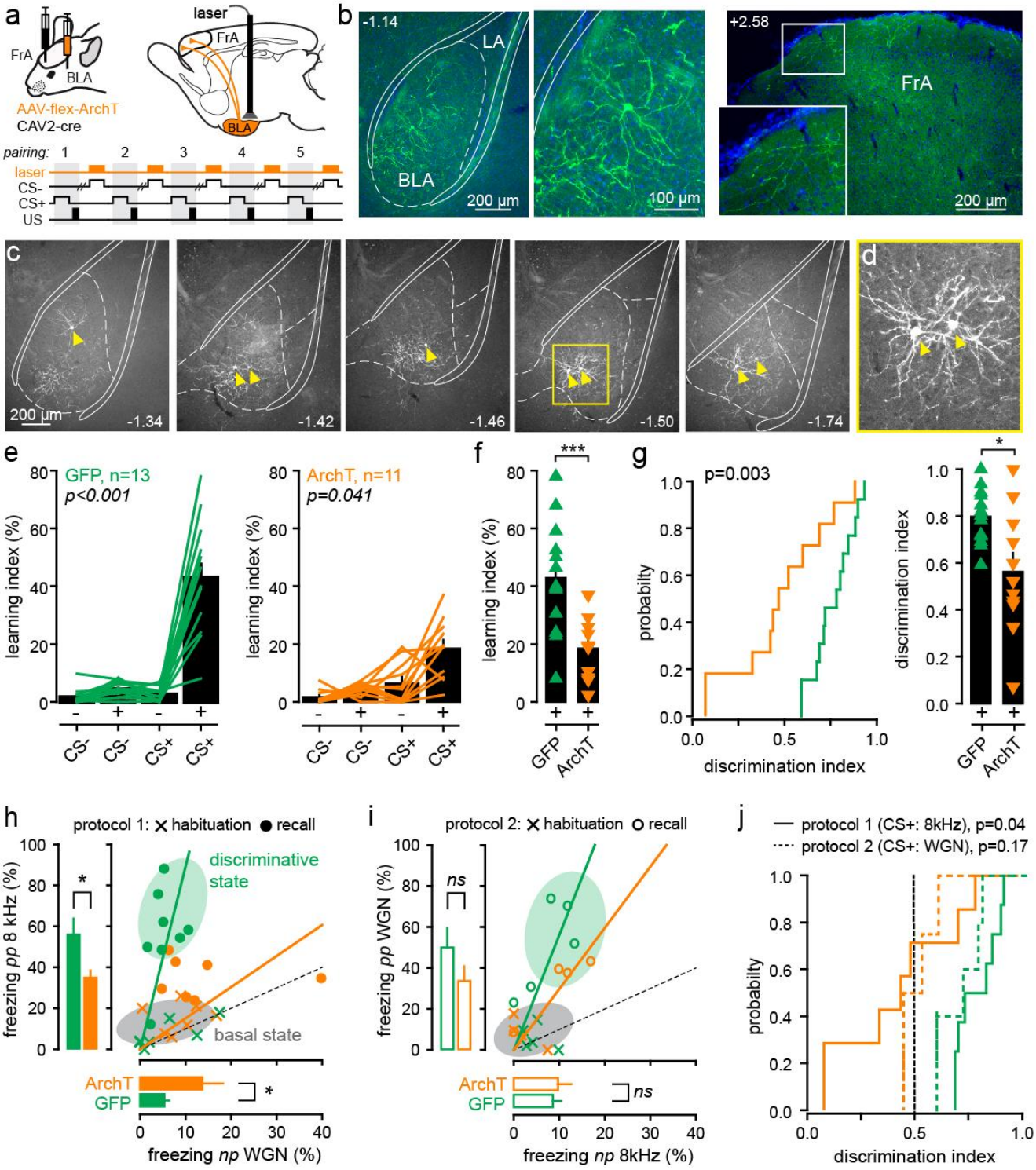


**Fig. 5**

**Figure 5. BLA-to-FrA projecting neurons mediate discriminative learning**

**a,** Experimental protocol. Mice were infected with AAV9-CBA-ArchT-Flex (or AAV9-CAG-flex-eGFP for controls) in BLA and CAV2-CMV-Cre in FrA, and chronically implanted with optical fibers in both BLA. BLA-to-FrA neurons expressing ArchT (or GFP) were then photo-stimulated during the presentation of CS-.

**b,** Example of expression profile of ArchT in BLA (left) and FrA (right). BLA, basolateral amygdala; LA, lateral amygdala.

**c, d,** Few neurons expressing ArchT were found throughout the entire BLA, but not the LA.

**e,** Effect of light on learning index during recall (+) as compared to habituation (-) in GFP-expressing mice (left; n=13, $p<0.001$, interaction, two-way repeated measures anova) and ArchT-expressing mice (right, n=11, $p=0.041$, interaction, two-way repeated measures anova). Green and orange lines represent individual mice.

**f,** Learning index quantified during CS+ in GFP- and ArchT-expressing mice ($p<0.001$, t-test). Triangles, individual mice.

**g,** The discrimination index is significantly higher in GFP-expressing mice as compared to ArchT-expressing mice during recall (left, $p=0.003$, Kolmogorov-Smirnov test; right, $p=0.016$, Mann-Whitney rank sum test).

**h,** Effect of light on freezing behaviors during recall upon pp8kHz (CS+ protocol 1; GFP vs ArchT, $p=0.037$, t-test) and npWGN (CS- protocol 1; GFP vs ArchT, $p=0.04$, t-test) presentation. The relation between 8kHz and WGN-evoked freezing during habituation (crosses) and recall (dotes) is also indicated.

**i,** Same presentation as in (H) but for ppWGN (CS+, protocol 2) and np8kHz (CS-, protocol 2). ns, $p>0.05$, t-test.

**j,** Distribution of discrimination index in GFP-expressing mice (green) and ArchT-expressing mice (orange) for protocol 1 (solid lines) and protocol 2 (dashed lines).

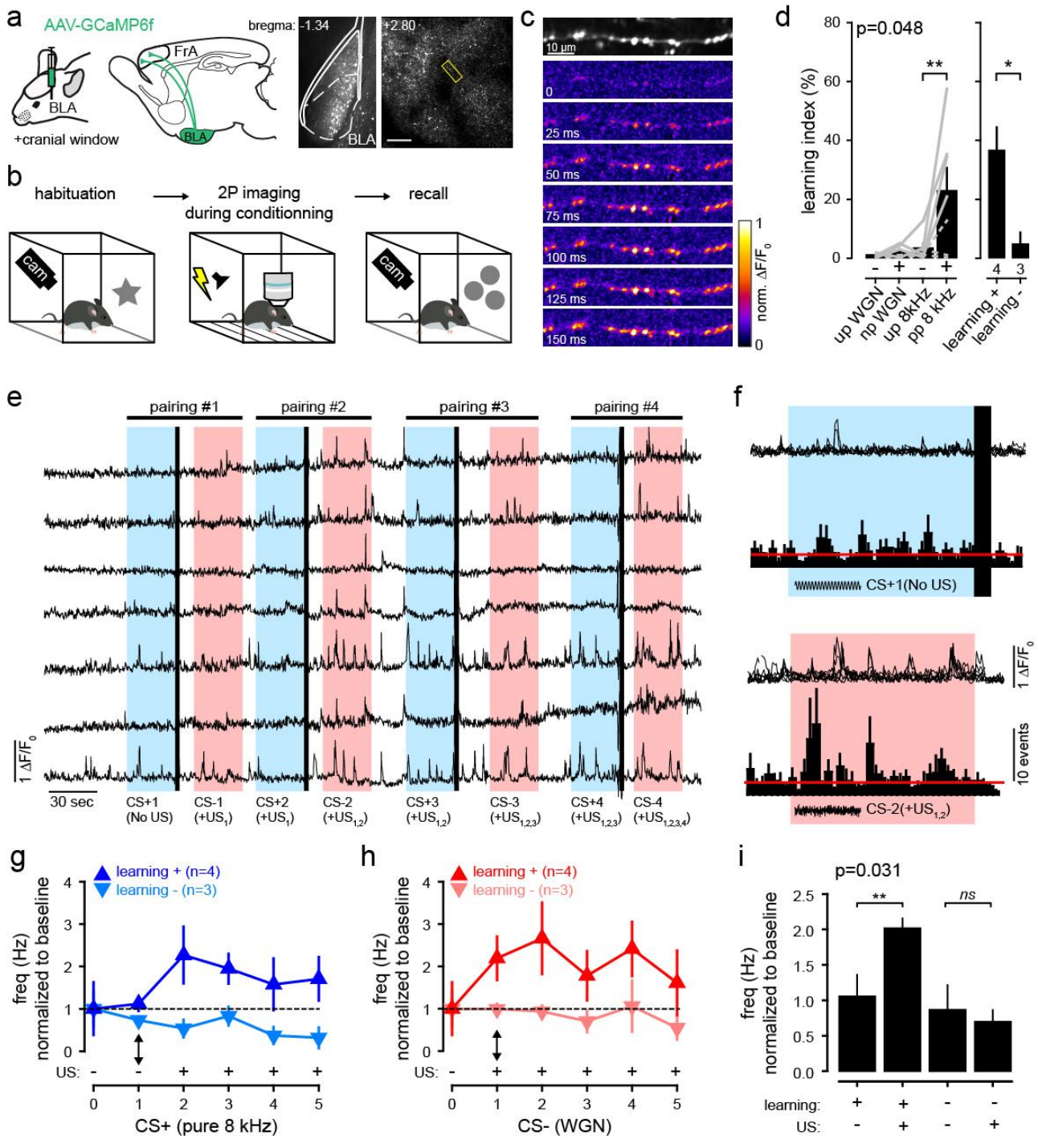


**Fig. 6**

**Figure 6. Activation of BLA-to-FrA axons during conditioning**

**a,** *Left*, experimental protocol. BLA neurons were transfected with AAV1-hSyn-GCAMP6f and their boutons were imaged in the superficial layer of the FrA. *Right*, expression profiles of GCaMP6f in the BLA (left) and FrA (middle). GCaMP6f-expressing axons (right) were imaged in the FrA of awake mice through a chronically-implanted cranial window (scale bar, 50 µm). PL, *prelimbic cortex*; IL, *infralimbic cortex*.

**b,** GCaMP6f-expressing mice were fear conditioned under the 2P microscope, and fear learning was quantified 24 h later in a new context.

**c,** Example of $Ca^{2+}$ transients in individual BLA-to-FrA axon.

**d,** *Left*, conditioning under the microscope induced robust fear behaviors (n=7; p=0.048, *two-way repeated measures anova*): in contrast to WGN, pure 8kHz tone increased fear learning index during recall (+) as compared to habituation (-) (**, p=0.003, *Holm-Sidak multiple comparisons*). Gray solid lines, learning index >20% (learning+, n=4); gray dashed lines, learning index <20% (learning-, n=3). *Right*, learning index induced by 8kHz during recall for learner (learning+) and non-learner (learning-) mice (p=0.026, *t-test*).

**e,** Examples of $Ca^{2+}$ transients ($\Delta F/F_0$) from individual boutons recorded from one mouse upon 4 consecutive CS+ / US pairings. Blue bars, *pp8kHz*; red bars, *npWGN*; black bars, footshock (US).

**f,** Examples of axonal $Ca^{2+}$ transients (*top*) and averaged histograms of distribution (± sem) (*bottom*, n=4 mice). Red lines, mean of events during baseline.

**g, h,** Frequency of axonal $Ca^{2+}$ transients recorded during successive *up* or *pp8kHz* (**g**) and *npWGN* (**h**). For the first CS+, the activity of boutons was monitored in absence of footshock (-). – and + points to as whether events were detected before (-) or after (+) the first footshock (US). Black arrow points to the difference between the first CS+ (before the first footshock) and the first CS- (after the first footshock). 0 corresponds to the baseline period before conditioning.

**i,** All events recorded during CS were pooled and averaged as a function of the presence (US+) or absence (US-) of the US, for learning (n=4) and non learning (n=3) mice. The effect of different levels of learning depends on whether the US is present or not (p=0.031, two-way anova). **, p=0.005 (Holm-Sidak multiple comparison).

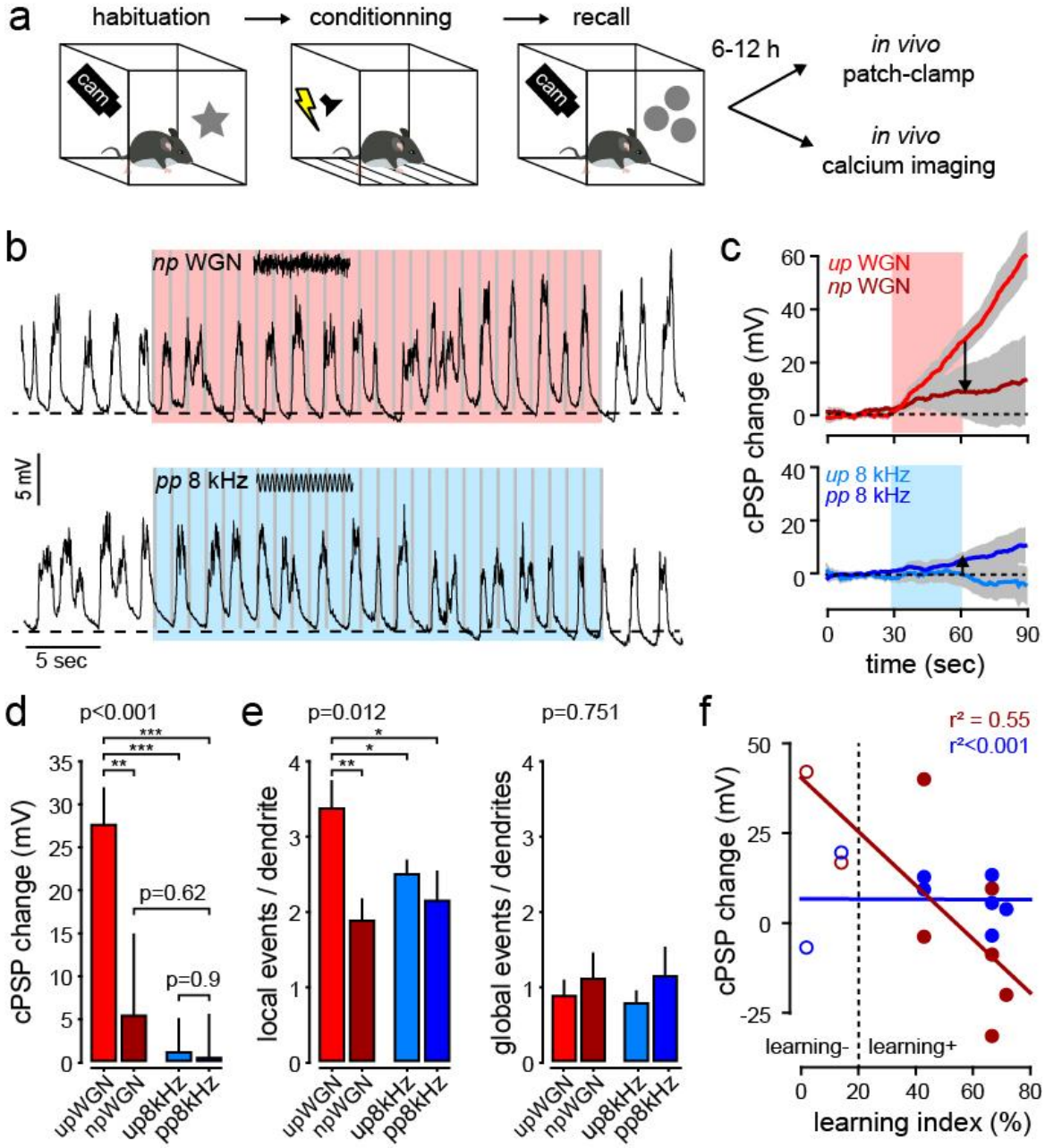


**Fig. 7**

**Figure 7. Fear conditioning occludes auditory-evoked plateau potentials**

**a,** Experimental protocol. Dendritic plateau potentials were assessed by 2P imaging (during wakefulness) and patch-clamp recording (during anesthesia) after fear conditioning (recall) upon *npWGN* (CS-) and *pp8kHz* (CS+) tone presentation.

**b,** Example traces of postsynaptic membrane potential recorded from an individual FrA pyramidal neuron upon *npWGN* (CS-, top) and *pp8kHz* (CS+, bottom) auditory stimulation. The effect of both stimuli was tested on the same cell.

**c,** Averaged cPSP change (± sem) evoked by WGN (top) and 8kHz tones (bottom) before (*upWGN, up8kHz*) and after (*npWGN, pp8kHz*) fear conditioning.

**d,** Effect of WGN and pure 8kHz tone on cPSP change before (WGN, red bar; 8kHz, blue bar; n=22) and after learning (WGN, dark red bar; 8kHz, dark blue bar; n=8). $p<0.001$, one-way anova; ***, $p<0.001$, **, $p<0.01$, Holm-Sidak comparisons.

**e,** The number of local (left) and global (right) events observed upon auditory stimulations before conditioning (WGN, red bar; 8kHz, blue bar, m=9) and after conditioning (WGN, dark red bar; 8kHz, dark blue bar, m=5). $p=0.012$, one way anova; *, $p<0.05$, **, $p<0.01$; Holm-Sidak comparisons.

**f,** Relation between the learning index and *npWGN* (red)- and *pp8kHz* (blue)-induced cPSP change after conditioning. Open / filled circles, individual cells from non-learning / learning mice, respectively.

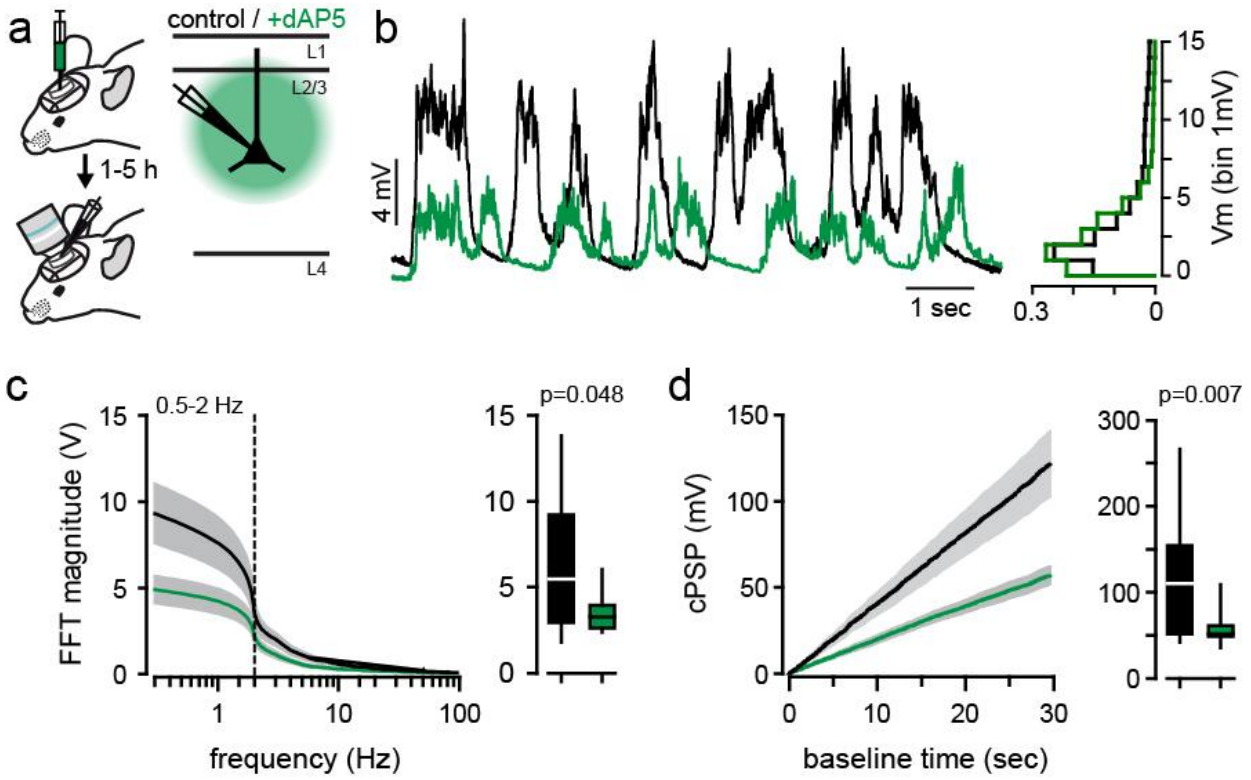


**Supplementary Fig. 1. Spontaneous membrane potential upon block of NMDARs with dAP5**

**a,** Experimental protocol: dAP5 (1µm) was applied ectopically through the dura and L2/3 pyramidal neurons were patched 1 to 5 hours later.

**b,** *Left*, examples of single-cell spontaneous membrane potential (Vm) fluctuations during anaesthesia in controls (black) and upon dAP5 injection (green). *Right*, corresponding membrane potential probability histograms.

**c,** *Left*, average (± sem) fast Fourier transform (FFT) of spontaneous membrane potentials in controls (black) and upon dAP5 injection (green). *Right*, blocking NMDARs significantly decreases the 0.5-2 Hz range in the FFT magnitude (p=0.048, Mann-Whitney rank sum test). Box plot represents median and interquartile range (control, n=22; dAP5, n=19).

**d,** *Left*, average (± sem) cumulative PSP (cPSP) of spontaneous membrane potentials in controls (black) and upon dAP5 injection (green). *Right*, blocking NMDARs significantly decreases the cPSP amplitude after 30 sec of recording (p=0.007, Mann-Whitney rank sum test). Box plot represents median and interquartile range (control, n=22; dAP5, n=19).

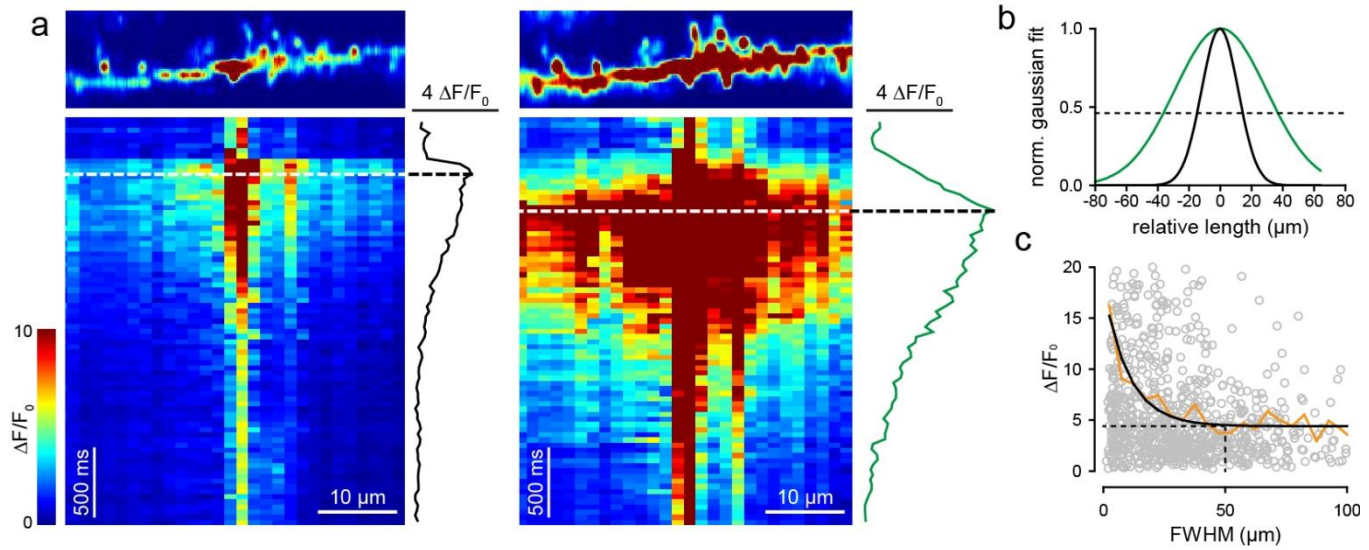


**Supplementary Fig. 2. Local and global calcium events in dendrites**

**a,** Example of single-dendrite local (*left*) and global (right) $Ca^{2+}$ events. *Bottom*, raster plot of $\Delta F/F_0$ for multiple ROIs along the dendrite represented above (aligned). *Right*, average $\Delta F/F_0$. Dashed line, time point of the maximum peak amplitude of averaged $\Delta F/F_0$.

**b,** Gaussian fits (normalized to max) of the local (black) and global (green) $Ca^2$ events shown in (**a**).

**c,** Relation between peak ΔF/F0 and fwhm for all detected events (including both local and global events). Circles, dendritic events. The yellow curve corresponds to the average ΔF/F0 of all events of a certain fwhm (bin of 5 µm). The black curve corresponds to the exponential fit of the yellow curve. The cut-off (50µm) corresponds to fwhm at which the exponential decay reaches the plateau.

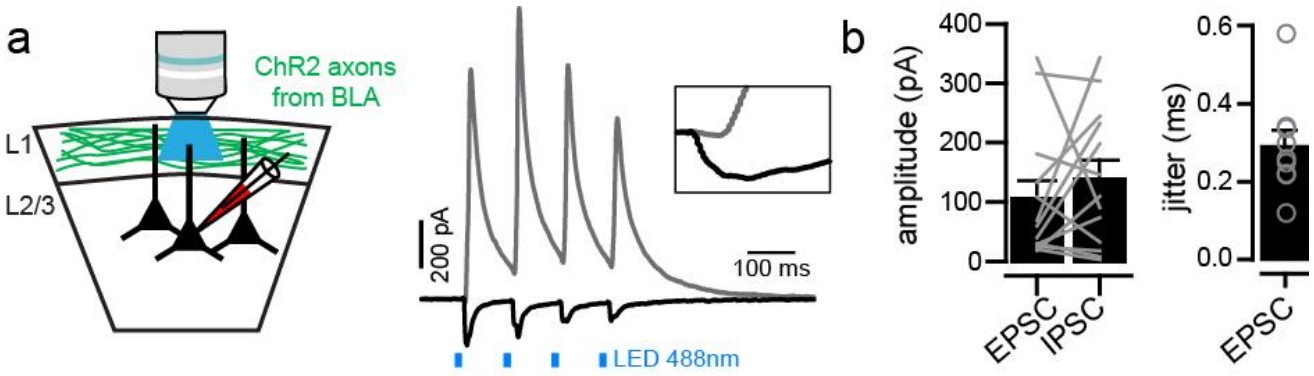


**Supplementary Fig. 3. BLA-mediated synaptic inputs onto FrA L2/3 pyramidal neurons in acute slices**

**a,** Schematic of the slice experiment. BLA-to-FrA axons expressing ChR2 were photo-activated through the objective. *Right*, representative examples of excitatory post-synaptic current (EPSCs) and feed-forward inhibitory post-synaptic currents (IPSCs) evoked on L2/3 pyramidal neurons with an ultrahigh power 488 nm LED.

**b,** Amplitude (*left*) and jitter (*right*) of light-evoked EPSCs. Gray lines indicate pairs. Open circles indicate individual cells.

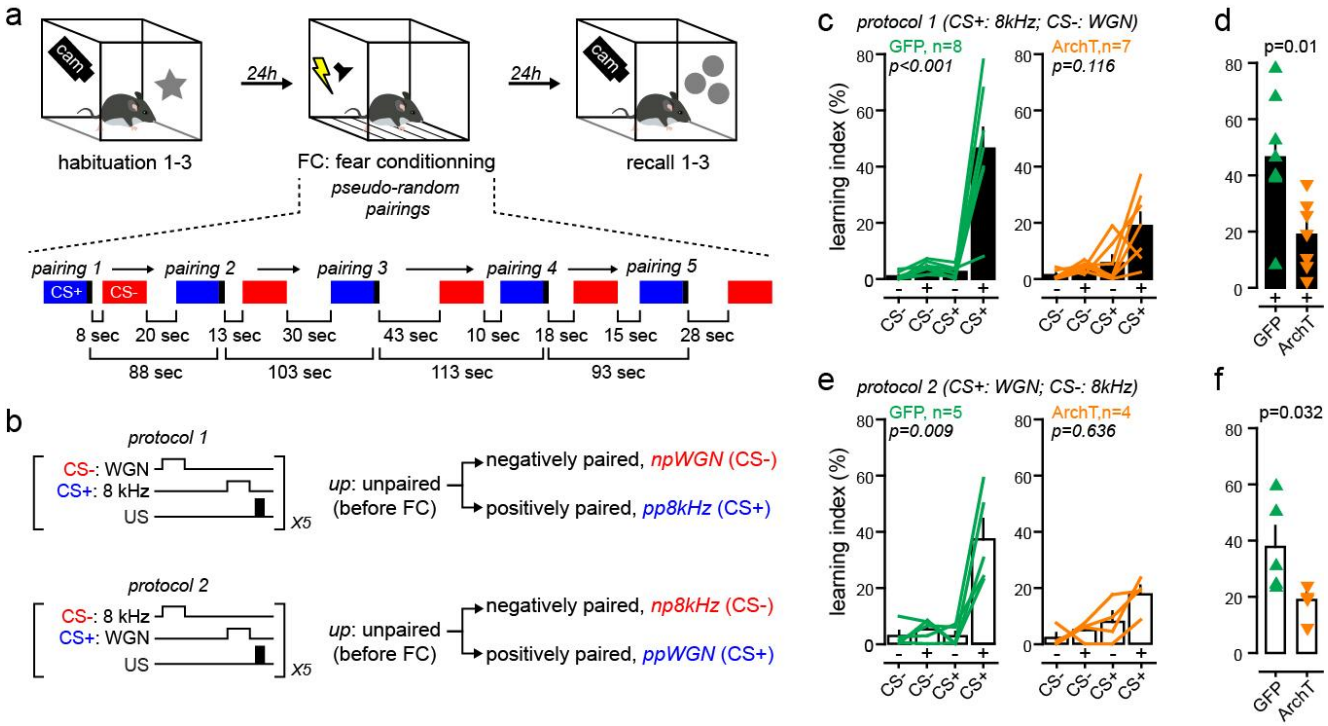


**Supplementary Fig. 4. Fear conditioning counterbalanced protocols**

**a,** Timeline of behavioral experiments. Pseudo-random delays between CS and between pairings are indicated below.

**b,** Fear conditioning protocols.

**c,** Effect of light on learning index (protocol 1) during recall (+) as compared to habituation (-) in GFP-expressing mice (left; n=8, p<0.001, interaction, two-way repeated measures anova) and ArchT-expressing mice (right, n=7, p=0.116, interaction, two-way repeated measures anova). Green and orange lines represent individual mice.

**d,** Learning index quantified during CS+ (protocol 1) in GFP- and ArchT-expressing mice (p=0.01, t-test). Triangles, individual mice.

**e, f,** same presentation as in (**c, d**), but for protocol 2.

| fig. | variable /units | group | N | M | norm. | mean | Std dev | median | 25% | 75% | test | p -value |
|---|---|---|---|---|---|---|---|---|---|---|---|---|
| 1e | upWGN cPSP change (mV) (time point1) | control | 22 | | passed | 27.617 | 19.741 | | | | One way anova | p<0.001 |
| | | dAP5 | 14 | | p=0.116 | -13.427 | 17.589 | | | | *with multiple comparisons* | *p<0.001 (control vs dAP5)* |
| | | iMK801 | 5 | | | -2.24 | 5.368 | | | | *(Holm-Sidak method)* | *p=0.002 (control vs iMK801)* |
| | upWGN cPSP change (mV) (time point 2) | control | 22 | | failed | | | 25.653 | 14.273 | 41.242 | Kruskal-Wallis one way anova on ranks | p<0.001 |
| | | dAP5 | 14 | | p<0.05 | | | -13.736 | -18.827 | -0.928 | *with multiple comparisons* | *p<0.05 (control vs dAP5)* |
| | | iMK801 | 5 | | | | | -0.263 | -15.97 | 4.812 | *(Dunn's method)* | *p<0.05 (control vs iMK801)* |
| 1f | up8kHz cPSP change (mV) (end of stimulation) | control | 22 | | passed | 1.16 | 18.145 | | | | One way anova | p=0.004 |
| | | dAP5 | 10 | | p=0.691 | -16.777 | 12.998 | | | | *with multiple comparisons* | *p=0.006 (control vs dAP5)* |
| | | iMK801 | 5 | | | -21.008 | 7.657 | | | | *(Holm-Sidak method)* | *p=0.008 (control vs iMK801)* |
| | up8kHz cPSP change (mV) (time point 2) | control | 22 | | passed | -3.823 | 14.122 | | | | One way anova | p=0.016 |
| | | dAP5 | 10 | | p=0.437 | -15.404 | 15.447 | | | | *with multiple comparisons* | *p=0.012 (control vs dAP5)* |
| | | iMK801 | 5 | | | -22.654 | 12.508 | | | | *(Holm-Sidak method)* | *p=0.041 (control vs iMK801)* |
| 2d,e | local events per dendrites (number) | baseline | | 9 | passed | 0.591 | 0.387 | | | | One way repeated measures anova | p<0.001 |
| | | upWGN | | 9 | p=0.796 | 3.371 | 1.082 | | | | *with multiple comparisons* | *p<0.001 (upWGN vs baseline)* |
| | | up8kHz | | 9 | | 2.497 | 0.532 | | | | *(Holm-Sidak method)* | *p<0.001 (up8kHz vs baseline)* |
| | | | | | | | | | | | | *p=0.011 (upWGN vs up8kHz)* |
| | Global events per dendrites (number) | baseline | | 9 | passed | 0.405 | 0.299 | | | | One way repeated measures anova | p=0.002 |
| | | upWGN | | 9 | p=0.842 | 0.881 | 0.61 | | | | *with multiple comparisons* | *p<0.001 (upWGN vs baseline)* |
| | | up8kHz | | 9 | | 0.786 | 0.469 | | | | *(Holm-Sidak method)* | *p<0.001 (up8kHz vs baseline)* |
| | | | | | | | | | | | | *p=0.429 (upWGN vs up8kHz)* |
| | fwhm of local events (µm) | baseline | 79 | | failed | | | 23.295 | 10.022 | 32.577 | Kruskal-Wallis one way anova on ranks | p=0.113 |
| | | upWGN | 338 | | p<0.05 | | | 18.536 | 7.39 | 32.772 | | |
| | | up8kHz | 253 | | | | | 22.648 | 12.046 | 32.701 | | |
| 3f | BLA-evoked PSP integral (mV*sec) | pre | 4 | | passed | 6.138 | 3.291 | | | | One way repeated measures anova | p=0.004 |
| | | hyper | 4 | | p=0.950 | 3.891 | 3.021 | | | | *with multiple comparisons* | *p=0.002 (pre vs hyper)* |
| | | post | 4 | | | 5.566 | 2.822 | | | | *(Holm-Sidak method)* | *p=0.007 (post vs hyper)* |
| | | | | | | | | | | | | *p=0.220 (post vs pre)* |
| 4b | upWGN cPSP change (mV) (time point1) | w/o light | 13 | | passed | 18.842 | 24.246 | | | | paired t-test | p=0.008 |
| | | w/light | 13 | | p=0.304 | 39.098 | 22.593 | | | | | |
| | upWGN cPSP change (mV) (time point2) | w/o light | 13 | | passed | 19.556 | 26.689 | | | | paired t-test | p=0.045 |
| | | w/light | 13 | | p=0.460 | 46.383 | 41.988 | | | | | |
| 4d | up8kHz cPSP change (mV) (time point1) | w/o light | 8 | | passed | -9.704 | 9.409 | | | | paired t-test | p<0.001 |
| | | w/light | 8 | | p=0.198 | 16.667 | 8.928 | | | | | |
| | up8kHz cPSP change (mV) (time point2) | w/o light | 8 | | passed | -10.882 | 15.645 | | | | paired t-test | p=0.013 |
| | | w/light | 8 | | p=0.905 | 14.846 | 18.769 | | | | | |

| fig. | variable /units | group | N | M | norm. | mean | Std dev | median | 25% | 75% | test | p -value |
|---|---|---|---|---|---|---|---|---|---|---|---|---|
| | cPSP change (mV) + light | upWGN | 13 | | failed | | | 48.968 | 15.389 | 61.042 | Mann-Whitney rank sum test | p=0.138 |
| | (time point1) | up8kHz | 8 | | p<0.05 | | | 18.567 | 14.746 | 22.133 | | |
| 4e | cPSP change (mV) + light | upWGN | 13 | | failed | | | 34.954 | 20.714 | 68.227 | Mann-Whitney rank sum test | p=0.039 |
| | (time point2) | up8kHz | 8 | | p<0.05 | | | 12.97 | -2.916 | 28.533 | | |
| | net BLA effect (mV)= | control | 13 | | passed | 20.256 | 23.11 | | | | t test | p<0.001 |
| | (cPSP w/ light)-(cPSP w/o light) | dAP5 | 7 | | p=0.524 | -30.165 | 18.278 | | | | | |
| | time point 1 | | | | | | | | | | | |
| 4g | net BLA effect (mV)= | control | 13 | | passed | 26.827 | 43.2 | | | | t test | p=0.004 |
| | (cPSP w/ light)-(cPSP w/o light) | dAP5 | 7 | | p=0.265 | -30.165 | 18.278 | | | | | |
| | time point 2 | | | | | | | | | | | |
| | learning index (%) | CS- hab | | 13 | failed | 1.7153 | 2.6984 | 0.5455 | | | Two way repeated measures anova | p<0.001 (interaction) |
| | GFP | CS- rec | | 13 | p<0.05 | 4.5547 | 2.6337 | 4.3718 | | | (two factor repetition) | *p<0.001 (CS+, rec vs hab)* |
| | hab=habituation | CS+ hab | | 13 | | 2.6028 | 2.5704 | 2.0029 | | | *with multiple comparisons* | *p=0.630 (CS-, rec vs hab)* |
| | rec=recall | CS+ rec | | 13 | | 42.925 | 19.201 | 39.9806 | | | *(Holm-Sidak method)* | *p=0.629 (hab, CS+ vs CS-)* |
| | | | | | | | | | | | | *p<0.001 (rec, CS+ vs CS-)* |
| 5e | learning index (%) | CS- hab | | 11 | failed | 1.7071 | 2.3456 | 0.6992 | | | Two way repeated measures anova | p=0.041 (interaction) |
| | ArchT | CS- rec | | 11 | p<0.05 | 4.4872 | 2.2704 | 4.8614 | | | (two factor repetition) | *p<0.001 (CS+, rec vs hab)* |
| | hab=habituation | CS+ hab | | 11 | | 6.4717 | 7.1515 | 4.4013 | | | *with multiple comparisons* | *p=0.329 (CS-, rec vs hab)* |
| | rec=recall | CS+ rec | | 11 | | 18.442 | 10.3461 | 19.2149 | | | *(Holm-Sidak method)* | *p=0.091 (hab, CS+ vs CS-)* |
| | | | | | | | | | | | | *p<0.001 (rec, CS+ vs CS-)* |
| | learning index (%) | GFP | | 13 | passed | 42.925 | 19.201 | | | | t -tet | p<0.001 |
| 5f | CS+ recall | ArchT | | 11 | p=0.999 | 18.442 | 10.346 | | | | | |
| | index of dicrimination= | GFP | | 13 | passed | | 0.792 | 0.689 | 0.886 | | Mann-Whitney rank sum test | p=0.012 |
| | (freezing CS+)-(freezing CS-) | ArchT | | 11 | p=0.637 | | 0.495 | 0.376 | 0.728 | | Kolmogorov-Smirnov test | p=0.003 |
| 5g | / (freezing CS+)+(freezing CS-) | | | | | | | | | | | |
| | recall | | | | | | | | | | | |
| | CS+: pp8kHz freezing (%) | GFP | | 8 | passed | 55.958 | 22.305 | | | | t-test | p=0.037 |
| | protocol 1 | ArchT | | 7 | p=0.208 | 34.905 | 9.337 | | | | | |
| 5h | CS-: npWGN freezing (%) | GFP | | 8 | failed | | | 5 | 3.167 | 7.083 | Mann-Whitney rank sum test | p=0.04 |
| | protocol 1 | ArchT | | 7 | p<0.05 | | | 10.167 | 6.708 | 14.125 | | |
| | CS+: ppWFN freezing (%) | GFP | | 5 | passed | 49.877 | 22.822 | | | | t-test | p=0.230 |
| | protocol 2 | ArchT | | 4 | p=0.208 | 32.132 | 15.857 | | | | | |
| 5i | CS-: np8kHz freezing (%) | GFP | | 5 | passed | 7.396 | 5.537 | | | | t-test | p=0.611 |
| | protocol 2 | ArchT | | 4 | p=0.591 | 9.619 | 7.054 | | | | | |

| fig. | variable /units | group | N | M | norm. | mean | Std dev | median | 25% | 75% | test | p -value |
|---|---|---|---|---|---|---|---|---|---|---|---|---|
| 5j | index of dicrimination= (freezing CS+)-(freezing CS-) / (freezing CS+)+(freezing CS-) recall protocol 1 | GFP | | 8 | passed | 0.8085 | 0.1013 | 0.832 | 0.704 | 0.893 | Mann-Whitney rank sum test | p=0.024 |
| | | ArchT | | 7 | p=0.742 | 0.5187 | 0.2802 | 0.469 | 0.351 | 0.748 | Kolmogorov-Smirnov test | p=0.04 |
| | recall protocol 2 | GFP | | 5 | passed | 0.7775 | 0.1491 | 0.782 | 0.682 | 0.851 | Mann-Whitney rank sum test | p=0.286 |
| | | ArchT | | 4 | | 0.6398 | 0.2489 | 0.56 | 0.48 | 0.799 | Kolmogorov-Smirnov test | p=0.17 |
| 6d | learning index (%) protocol 1 | upWGN | | 7 | failed | 0.4794 | 0.8901 | | | | Two way repeated measures anova (two factor repetition) *with multiple comparisons (Holm-Sidak method)* | p=0.048 (interaction) *p=0.688 (upWGN vs up8kHz)* *p=0.003 (npWGN vs pp8kHz)* *p=0.853 (upWGN vs npWGN)* *p=0.003 (up8kHz vs pp8kHz)* |
| | | up8kHz | | 7 | p<0.05 | 2.8301 | 4.4846 | | | | | |
| | | npWGN | | 7 | | 1.7599 | 2.0677 | | | | | |
| | | pp8kHz | | 7 | | 22.597 | 20.8057 | | | | | |
| | pp8kHz learning index (%) | learning+ | | 4 | passed | 36.192 | 16.076 | | | | t-test | p=0.026 |
| | | learning- | | 3 | p=0.265 | 4.471 | 6.965 | | | | | |
| 6i | events/axon (number) frequency normalized to baseline | learning+ /US- | 8 | | failed p<0.05 | 1.0573 | 0.2275 | 1 | 0.967 | 1.136 | Two way anova (two factor repetition) *with multiple comparisons (Holm-Sidak method)* | p=0.031 (interaction) *p=0.005 (learning+, US- vs +)* *p=0.667 (learning-, US- vs +)* *p=0.678 (US-, learning+ vs -)* *p<0.001 (US+, learning+ vs -)* |
| | | learning+ /US+ | 36 | | | 2.0156 | 1.1567 | 1.518 | 1.169 | 3.121 | | |
| | | learning- /US- | 6 | | | 0.8645 | 0.1718 | 0.908 | 0.8 | 1 | | |
| | | learning- /US+ | 27 | | | 0.6976 | 0.4862 | 0.787 | 0.257 | 0.895 | | |
| 7d | cPSP change (mV) time point 1 before/after learning protocol 1 | upWGN | 22 | | passed | 27.617 | 19.741 | | | | one-way anova *with multiple comparisons (Holm-Sidak method)* | p<0.001 *p=0.008 (upWGN vs npWGN)* *p<0.001 (upWGN vs up8kHz)* *p<0.001 (upWGN vs pp8kHz)* *p=0.601 (npWGN vs up8Khz)* *p=0.620 (npWGN vs pp8Khz)* *p=0.938 (np8kHz vs pp8kHz)* |
| | | npWGN | 8 | | p=0.549 | 1.16 | 18.145 | | | | | |
| | | up8kHz | 22 | | | 5.407 | 26.645 | | | | | |
| | | pp8kHz | 8 | | | 0.526 | 14.083 | | | | | |
| 7e | local events per dendrites (number) | upWGN | | 9 | passed | 3.371 | 1.082 | | | | one-way anova *with multiple comparisons (Holm-Sidak method)* | p=0.012 *p=0.003 (upWGN vs npWGN)* *p=0.033 (upWGN vs up8kHz)* *p=0.013 (upWGN vs np8kHz)* |
| | | npWGN | | 5 | p=0.645 | 1.882 | 0.623 | | | | | |
| | | up8kHz | | 9 | | 2.497 | 0.532 | | | | | |
| | | pp8kHz | | 5 | | 2.145 | 0.866 | | | | | |
| | global events per dendrites (number) | upWGN | | 9 | passed | 0.881 | 0.61 | | | | one-way anova | p=0.751 |
| | | npWGN | | 5 | p=0.272 | 1.108 | 0.741 | | | | | |
| | | up8kHz | | 9 | | 0.809 | 0.496 | | | | | |
| | | pp8kHz | | 5 | | 1.143 | 0.837 | | | | | |

| fig. | variable /units | group | N | M | norm. | mean | Std dev | median | 25% | 75% | test | p -value |
|---|---|---|---|---|---|---|---|---|---|---|---|---|
| | FFT magnitude (V) | ctrl | 22 | | failed | | | 5.452 | 2.967 | 9.072 | Mann-Whitney rank sum test | p=0.048 |
| s1c | 0.5-2Hz | dAP5 | 19 | | p<0.05 | | | 3.26 | 2.651 | 3.919 | | |
| | spontaneaous 30s-cumulative | ctrl | 22 | | failed | | | 110.386 | 52.252 | 148.21 | Mann-Whitney rank sum test | p=0.007 |
| s1d | potential (mV) | dAP5 | 19 | | p<0.05 | | | 51.515 | 48.765 | 61.167 | | |
| | learning index (%) | upWGN | | 8 | failed | -0.1628 | 1.7392 | 0.396 | 0 | 1.785 | Two way repeated measures anova | p<0.001 (habituation vs recall) |
| | GFP expressing mice | up8kHz | | 8 | p<0.05 | 2.0378 | 2.6342 | 2.751 | 0.604 | 3.833 | (two factor repetition) | p<0.001 (WGN vs 8kHz) |
| | protocol 1 | npWGN | | 8 | | 4.1861 | 2.0421 | 4.163 | 2.586 | 5.54 | *with multiple comparisons* | p=0.001 (interaction) |
| | | pp8kHz | | 8 | | 46.418 | 21.0604 | 43.211 | 39.261 | 60.182 | *(Holm-Sidak method)* | *p=0.772 (upWGN vs up8kHz)* |
| | | | | | | | | | | | | *p<0.001 (npWGN vs pp8kHz)* |
| | | | | | | | | | | | | *p=0.569 (upWGN vs npWGN)* |
| s4c | | | | | | | | | | | | *p<0.001 (up8kHz vs pp8kHz)* |
| | learning index (%) | upWGN | | 7 | failed | 1.2703 | 1.8187 | 0.699 | 0.491 | 2.617 | Two way repeated measures anova | p=0.031 (habituation vs recall) |
| | ArchT expressing mice | up8kHz | | 7 | p<0.05 | 5.4916 | 7.5535 | 1.154 | 0.546 | 10.836 | (two factor repetition) | p=0.009 (WGN vs 8kHz) |
| | protocol 1 | npWGN | | 7 | | 3.4585 | 3.2187 | 4.316 | 3.125 | 5.262 | *with multiple comparisons* | p=0.116 (interaction) |
| | | pp8kHz | | 7 | | 18.184 | 12.549 | 19.215 | 8.477 | 28.424 | *(Holm-Sidak method)* | |
| | learning index (%) | GFP | | 8 | passed | 46.418 | 21.06 | | | | t-test | p=0.01 |
| s4d | pp8kHz | ArchT | | 7 | p=0.856 | 18.892 | 12.549 | | | | | |
| | learning index (%) | up8kHz | | 5 | failed | 2.8546 | 3.9843 | 1.33 | 0.406 | 4.308 | Two way repeated measures anova | p=0.013 (habituation vs recall) |
| | GFP expressing mice | upWGN | | 5 | p<0.05 | 2.7057 | 3.4984 | 0.339 | 0.127 | 6.228 | (two factor repetition) | p=0.013 (WGN vs 8kHz) |
| | protocol 2 | np8kHz | | 5 | | 5.1444 | 3.5783 | 6.522 | 2.203 | 7.999 | *with multiple comparisons* | p=0.009 (interaction) |
| | | ppWGN | | 5 | | 37.337 | 16.3221 | 30.623 | 23.752 | 52.317 | *(Holm-Sidak method)* | *p=0.979 (upWGN vs up8kHz)* |
| | | | | | | | | | | | | *p<0.001 (ppWGN vs np8kHz)* |
| | | | | | | | | | | | | *p=0.979 (up8kHz vs np8kHz)* |
| s4f | | | | | | | | | | | | *p<0.001 (upWGN vs ppWGN)* |
| | learning index (%) | up8kHz | | 4 | failed | 2.118 | 3.5584 | 0.535 | 0 | 4.236 | Two way repeated measures anova | p=0.049 (habituation vs recall) |
| | ArchT expressing mice | upWGN | | 4 | p<0.05 | 7.8737 | 7.5441 | 6.964 | 2.201 | 13.547 | (two factor repetition) | p=0.049 (WGN vs 8kHz) |
| | protocol 2 | np8kHz | | 4 | | 4.8586 | 3.3028 | 6.026 | 2.955 | 6.762 | *with multiple comparisons* | p=0.636 (interaction) |
| | | ppWGN | | 4 | | 17.654 | 6.3694 | 19.228 | 13.76 | 21.548 | *(Holm-Sidak method)* | |
| | learning index (%) | GFP | | 5 | passed | 37.337 | 16.322 | 30.623 | 23.752 | 52.317 | t-test | p=0.059 |
| s4e | ppWGN | ArchT | | 4 | p=0.856 | 17.654 | 6.369 | 19.228 | 13.76 | 21.548 | Mann-Whitney rank sum test | p=0.032 |